

# Data-Driven Prediction of CRISPR-Based Transcription Regulation for Programmable Control of Metabolic Flux

Jiayuan Sheng<sup>†</sup>, Weihua Guo<sup>†</sup>, Christine Ash, Brendan Freitas, Mitchell Paoletti, and Xueyang Feng<sup>\*</sup>

Department of Biological Systems Engineering, Virginia Polytechnic Institute and State University, Blacksburg, VA 24061

<sup>†</sup> WG and JS are equally contributed.

\* To whom correspondence should be addressed. X.F: Phone: (540) 231-2974. E-mail: xueyang@vt.edu.

**Abstract.** Multiplex and multi-directional control of metabolic pathways is crucial for metabolic engineering to improve product yield of fuels, chemicals, and pharmaceuticals. To achieve this goal, artificial transcriptional regulators such as CRISPR-based transcription regulators have been developed to specifically activate or repress genes of interest. Here, we found that by deploying guide RNAs to target on DNA sites at different locations of genetic cassettes, we could use just one synthetic CRISPR-based transcriptional regulator to simultaneously activate and repress gene expressions. By using the pairwise datasets of guide RNAs and gene expressions, we developed a data-driven predictive model to rationally design this system for fine-tuning expression of target genes. We demonstrated that this system could achieve programmable control of metabolic fluxes when using yeast to produce versatile chemicals. We anticipate that this master CRISPR-based transcription regulator will be a valuable addition to the synthetic biology toolkit for metabolic engineering, speeding up the “design-build-test” cycle in industrial biomanufacturing as well as generating new biological insights on the fates of eukaryotic cells.

## Introduction

Metabolic engineering has proven to be tremendously important for sustainable production of fuels<sup>1, 2</sup>, chemicals<sup>3, 4</sup>, and pharmaceuticals<sup>5, 6</sup>. One of the critical steps in metabolic engineering is reprogramming metabolic fluxes in host cells to optimize the fermentation performance such as product yield<sup>7, 8</sup>. To achieve this goal, several enzymes need to be activated while in the meantime others need to be repressed<sup>9</sup>. The multiplex and multi-directional control of enzyme expressions is largely executed through transcriptional regulation<sup>9-12</sup>. Recently, the type-II clustered regularly interspaced short palindromic repeats (CRISPR)/Cas9 from *Streptococcus pyogenes* (*Sp*)<sup>13-15</sup> has been repurposed to be a master transcriptional regulator that could activate or repress multiple genes<sup>16-18</sup>. By further extending the guide RNAs of SpCas9 to include effector protein recruitment sites and expressing the effector proteins in host cells<sup>18, 19</sup>, a synthetic CRISPR-based transcriptional regulator was developed to simultaneously program the expressions of multiple genes at multiple directions (i.e., both activation and repression).

Although demonstrating great promises in controlling metabolic fluxes, the current CRISPR-based transcription regulation faces several challenges when being applied for metabolic engineering. First, it relies on a panel of well-characterized genetic parts (e.g., RNA-binding proteins) to achieve the transcriptional regulation<sup>9, 20</sup>. However, the rareness of such genetic parts often limits the application of current CRISPR-based transcription regulator in a metabolic network. Second, it requires the co-expression of effector proteins to activate or repress the target genes<sup>9, 20</sup>. Therefore, the utility of current CRISPR-based transcription regulator in metabolic engineering is mitigated by the metabolic costs associated with protein expressions<sup>9, 20</sup>. To address these limitations, an ideal type of CRISPR-based transcription regulation should meet two criteria: generally applicable in any gene of interest, and requiring minimal protein expression to achieve multi-directional gene regulation.

In this study, we have developed a data-driven approach that enables the rational design of a new type of CRISPR-based transcription regulation. This CRISPR-based transcription regulator uses only a fused protein of a nuclease-deficient Cas9 (dCas9) and an effector (VP64) to achieve multi-directional and multiplex gene regulation, which eliminates the metabolic costs associated with the expression of effector proteins in previous studies<sup>9, 20</sup>. We found that the deployment of guide RNAs was the key factor that determined the regulatory effects of our CRISPR-based transcription regulator. We used a data-driven approach to

provide accurate and target-oriented guidance on designing the guide RNAs. As we showed in our results, this approach could be applied for any gene of interest. Finally, using this system, we demonstrated a highly programmable control of metabolic fluxes when using yeast to produce versatile chemicals.

## Results

**Gene activation and repression by using a CRISPR-based transcriptional regulator.** The CRISPR-based transcriptional regulator is composed of a codon-optimized, catalytically dead SpCa9 (i.e., dCas9) that is fused with four tandem copies of Herpes Simplex Viral Protein 16 (VP64, a commonly used eukaryotic transcription activator domain). The similar molecular design was previously reported to be able to activate gene expression in yeast<sup>18</sup> and mammalian cells<sup>18</sup>. In brief, it was found that when the dCas9-VP64 regulator was positioned in the correct sites of promoter, the target gene could be activated by the VP64. However, we hypothesized that the effects of dCas9-VP64 could be diverse, i.e., both activation and repression could be achieved by using this master regulator (Fig. 1A). For example, the transcription initiation could be blocked when dCas9-VP64 is deployed to the transcription starting sites (TSS). The transcription elongation could also be inhibited when dCas9-VP64 is deployed to the open reading frame (ORF). If the hypothesis stands, we could then repurpose dCas9-VP64 as a universal regulator to activate and repress gene expressions at the same time.

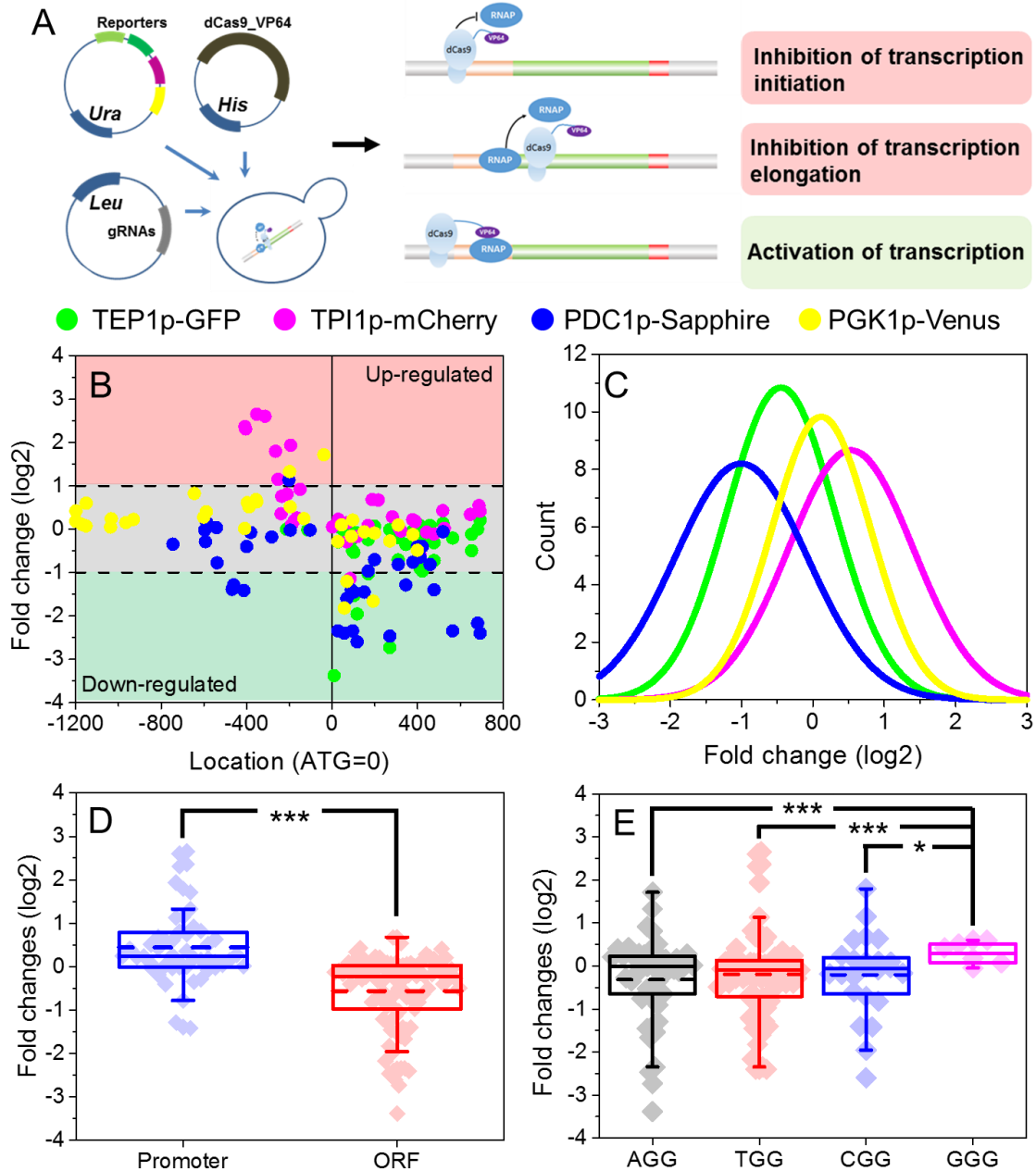


**Figure 1.** Multi-directional transcriptional regulation by dCas9-VP64. (A) Hypothesized mechanism of transcriptional regulation by dCas9-VP64 to achieve both gene activation and gene repression. (B) The measured fold changes of gene expressions from the four synthetic genetic cassettes based on the PAM position. (C) The distributions of fold changes of gene expressions. (D) Comparison of fold changes of gene expressions from two groups: PAM sites located in the promoter regions and PAM sites located in the ORF region. \*\*\*:  $p < 0.01$ . (E) Effects of different PAM sites on transcriptional regulation by dCas9-VP64. \*:  $p < 0.05$ .

To validate our hypothesis, we designed experiments by selecting 138 sites that can be targeted by dCas9-VP64 in four synthetic

genetic cassettes (Fig. 1B): GFP under TEF1p promoter, mCherry under TPI1p promoter, Sapphire under PGK1p promoter, and Venus

under PDC1p promoter. We created a library of guide RNAs and co-expressed them with the dCas9-VP64 and the target genetic cassette. For each of the tests, we measured the fluorescence of the reporter proteins and compared it to a control test in which dCas9-VP64 and the genetic cassette were expressed without guide RNA. As summarized in Fig. 1B and Fig. 1C, expression of reporter genes could indeed be programmed to be either up- or down-regulated (cutoff fold-change set as two-fold,  $p<0.05$ ) when positioning the guide RNA at different sites on the promoter or ORF. The dynamic range of transcriptional regulation via dCas9-VP64 varied for different genetic elements, with the largest dynamic range achieving 13.8-fold (from -1.14 to 2.65 of log<sub>2</sub> gene fold-change) in expression of TPI1p-mCherry cassette and the smallest log<sub>2</sub> fold change dynamic range achieving 11.6-fold (from -1.82 to 1.71 of log<sub>2</sub> gene fold-change) in expression of PGK1p-Venus cassette. We next compared the effects on transcriptional regulation when guide RNAs were positioned in the promoter region to that were positioned in the gene region (Fig. 1D). A significant difference ( $p<0.01$ ) was revealed: while gene expression was in general down-regulated when guide RNAs were positioned in the gene region, most of the guide RNAs (94.2%) that were positioned in the promoter region led to gene up-regulation or no effect. We also evaluated whether different PAM sites (i.e., 3'AGG, 3'TGG, 3'CGG, 3'GGG) could bias the transcriptional regulation (Fig. 1E). We found that most of the PAM sites (3'AGG, 3'TGG, 3'CGG) have no bias, but when guide RNAs were targeted on 3'GGG sites, the expression of selected genes tends to be more up-regulated than other PAM sites ( $p<0.05$ ). Such difference, as we discussed

in the section below, may be attributed to the larger percentage of guanosine in 3'GGG sites. Finally, we evaluated the metabolic costs of dCas9-VP64 by comparing the growth rates of yeast between the ones subject to transcriptional regulation (i.e., with guide RNAs) and the ones that were not. As shown in Fig. S1, 131 out of the 138 tests showed no significant difference ( $p>0.05$ ) on cell growth rate when being compared to that of the control strain, indicating a minimal metabolic burden when using only one synthetic protein for transcriptional regulation.

**Data-driven model of transcriptional regulation by using dCas9-VP64.** To determine the rule underlying transcriptional regulation by dCas9-VP64, we solicited nine design parameters on nucleotide stability, sequence of the target genetic element, PAM site location, and protein-DNA structure. These design parameters were chosen based on previous studies on the activity of SpCas9<sup>21,22</sup>. Next, we correlated these design parameters with transcriptional regulation (Fig. S2A), and calculated the Pearson's correlation coefficients (PCC). The top 3 correlated design parameters were location, GC content (GC%), and PAM site of GGG. Next, we aimed to develop a predictive model that could use the design parameters to describe the effects of guide RNAs positioning on gene expressions. Our first attempt is a linear regression model, which utilized all the nine design parameters (i.e., GC%, location, number of base G, number of base A, ΔG, AGG, TGG, CGG, and GGG) to simulate the corresponding fold changes of gene expressions as we collected from the four synthetic genetic cassettes (Fig. S2B). However, the fitting of the linear regression model was

very bad, as demonstrated by the low PCC (0.41) between observed and simulated fold changes (Fig. S2B). This clearly indicated that the

biomolecular interactions of RNA-protein and DNA-protein in the dCas9-VP64 system were highly nonlinear, which cannot be captured by the simple linear regression model.

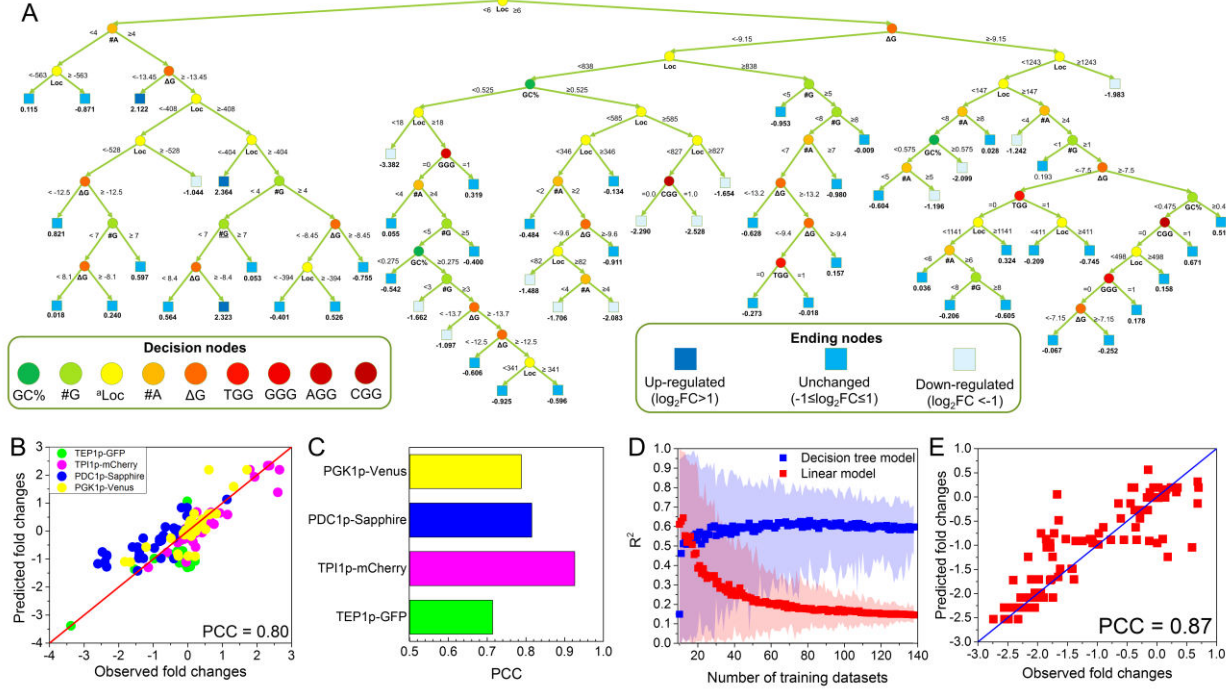


**Figure 2.** Data-driven model of transcriptional regulation by using dCas9-VP64. (A) Binary regression tree model trained with all the screening data from the four synthetic genetic cassettes. The regression tree model consisted of 58 decision nodes and used six design parameters of guide RNAs as input. (B) and (C) Prediction accuracy of the regression tree model from ten-fold cross validation. (D) Impact of data size on model prediction. For data-driven model, the prediction increased with the inclusion of more datasets. For linear model, the prediction decreased when more datasets were used. The shadow areas indicate the 95% confidence interval of model prediction. (E) Validation of the regression tree model by comparing the simulated and experimentally measured gene regulations on Eno2p-tdTomato cassette subject to dCas9-VP64 regulation.

We then used machine learning to derive an empirical model to quantitatively predict the nonlinear correlation between design parameters and transcriptional regulation by dCas9-VP64. As a data-driven modeling approach, machine learning is advantageous than linear model in solving complex problems in two aspects<sup>23-25</sup>: requiring no *a priori* knowledge of the system, and capable of resolving complex systems with high non-

linearity and multi-dimensionality. In this study, we used the pairwise data of the design parameters of guide RNAs and the corresponding fold-change of gene expressions to train the computer for developing a mathematical model that could accurately predict the causal effects of inputs (i.e., regulated gene expression in this study). We used decision tree method to build a machine-learning algorithm and adopted ten-fold cross

validation to evaluate the prediction accuracy of our model (Fig. 2A). The model construction and model evaluation were conducted by following a toolkit developed in MATLAB™ (i.e., “*fittree*” and “*predict*” in Statistics and Machine Learning Toolbox), which automatically adjust the nodes and connections of the decision tree to optimize the fitting<sup>26, 27</sup>. Using the 138 pairwise data collected from the synthetic genetic cassettes (i.e., TEF1p-GFP, TPI1p-mCherry, PDC1p-Sapphire, and PGK1p-Venus), we found that the prediction accuracy was dramatically improved with PCC reaching 0.80 (Fig. 2B) for overall prediction of gene regulation and 0.72~0.93 for predicting gene regulation of individual genetic cassettes (Fig. 2C). Also, we found that the prediction accuracy of our machine-learning algorithm was improved with the enlargement of data size (Fig. 2D). For example, when 20 pairwise datasets were chosen, the PCC was merely 0.66. However, when the number of pairwise datasets reached 80, the PCC was improved to 0.78. This demonstrated the unique advantage of data-driven algorithm, i.e., increased prediction accuracy with more data.

To further test if our machine-learning algorithm could be generally applied for predicting the transcriptional regulation of other genes, we designed another synthetic genetic cassette that expressed tdTomato under Eno2p promoter. We used the machine-learning algorithm to predict the regulated gene expressions when guide RNAs of dCas9-VP64 were positioned at different locations of Eno2p-tdTomato cassette, followed by constructing the genetic cassettes and conducting experimental measurements. Of the 99 guide RNAs tested, our machine-learning algorithm could achieve

similarly high prediction accuracy with PCC between the predicted and the measured gene expressions reaching 0.87 (Fig. 2E). This success demonstrated that our data-driven model could be generally applicable to guide the biomolecular design of dCas9-VP64 system to achieve customized gene regulation.

We also packaged our machine-learning algorithm into an open-source toolbox (Fig. S3 and supplementary software), CRISTINES (CRISPR-Cas9 Transcriptional Inactivation aNd Elevation System), which is a MATLAB-based toolbox and free for downloading at <https://sites.google.com/a/vt.edu/biomolecular-engineering-lab/software>. CRISTINES is able to analyze the input DNA sequences, identify the design parameters of the dCas9-VP64 system, and use the embedded decision-tree algorithm to provide the top five guide RNAs that would lead to the strongest up-regulation and down-regulations, respectively. We anticipated that CRISTINES could help biologists worldwide to customize their design based on the target gene of interest.

**Design dCas9-VP64 to reprogram metabolic fluxes in yeast.** We next applied dCas9-VP64 system in yeast metabolic engineering to test if the metabolic fluxes could be flexibly reprogrammed using our CRISPR-based transcription regulator. We chose the highly branched bacterial violacein biosynthetic pathway as our model pathway<sup>28</sup> (Fig. 3A), which uses five enzymes (VioA, VioB, VioE, VioD, and VioC) to produce four high-value products (violacein, proviolacein, deoxyviolacein, and prodeoxyviolacein). By controlling the expression levels of the five enzymes, the metabolic fluxes flowing into

different branch pathways could be varied and thus leading to different yield of the four products. In this study, we reconstituted the violacein pathway in yeast by expressing the five enzymes under constitutive promoters (i.e., TEF1p, PGK1p, ENO2p, TPI1p, and PDC1p). According to our data-driven model CRISTINES, we could computationally predict the gene expression and thus predict the metabolic fluxes in the violacein pathway. Here, we designed three guide RNAs for four genes

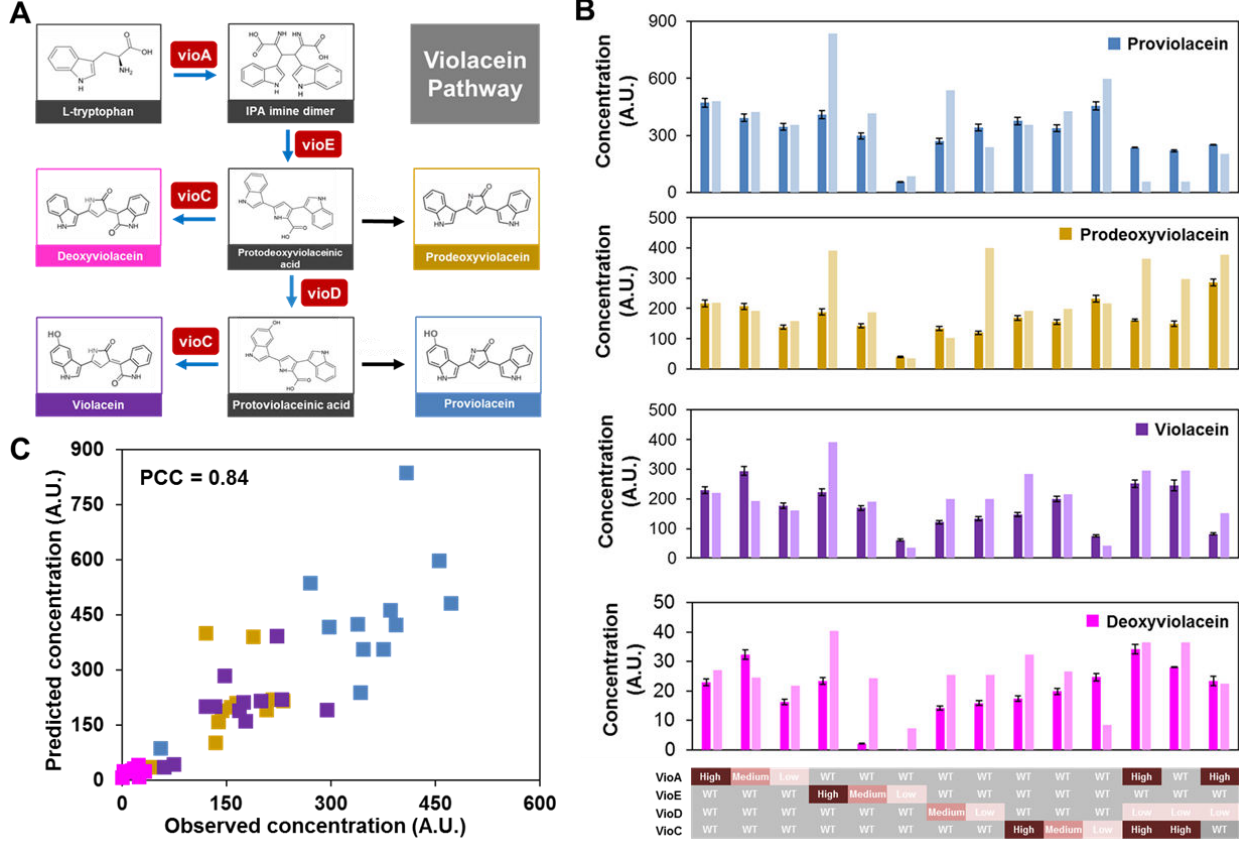


**Figure 3.** Design dCas9-VP64 to reprogram metabolic fluxes in yeast. (A) Violacein pathway in yeast used in this study to demonstrate the programmable control of metabolic fluxes by using dCas9-VP64. Five enzymatic steps (vioA, vioB, vioC, vioD, and vioE) and two non-enzymatic steps led to four products from the violacein pathway: proviolacein, prodeoxyviolacein, violacein, and deoxyviolacein. (B) A panel of genes subject to regulation of dCas9-VP64 were chosen to control metabolic fluxes to various products from the violacein pathway. WT: wild type gene without any regulation; High: highly up-regulated gene expression by dCas9-VP64; Medium: medium-level up-regulated gene expression by dCas9-VP64; Low: down-regulated gene expression by dCas9-VP64. (C) The compassion between the model-predicted and experimentally measured products from the violacein pathway. The high correlation coefficient ( $PCC=0.84$ ) indicated that the data-driven model could accurately predict the effects of artificial Cas9-based regulator on metabolic flux reprogramming.

our predictions on metabolic flux reprogramming, we co-expressed the dCas9-VP64 system with the violacein pathway, and used various guide RNAs to fine tune gene expressions. For each of the tests, we measured the titer of violacein, proviolacein, deoxyviolacein, and prodeoxyviolacein produced by yeast. As shown in Fig. 3B and 3C, our prediction fit well with the experimental measurements, with PCC reaching 0.84. We noticed some of the predictions on metabolic fluxes were not as good as we expected. This could be attributed to the posttranscriptional regulation of the five enzymes in the violacein pathway. Overall, we demonstrated that our master CRISPR-based transcription regulator was indeed able to program metabolic fluxes. More importantly, our data-driven algorithm allows users to design metabolic pathways with deterministic fates *in silico*.

## Discussion

Using data-driven approach to investigate biomolecular interactions of CRISPR-based systems has recently been showcased in several studies, such as rational design of guide RNAs for maximizing editing activity and minimizing off-target effects of SpCas9<sup>29,30</sup>. This approach is advantageous compared to conventional deterministic models because it does not require *a priori* knowledge on the mechanisms of RNA-protein and DNA-protein interactions<sup>31,32</sup>, which still remains largely unknown in spite of numerous studies on SpCas9 structures<sup>33-37</sup>. Also, because the biomolecular interactions among Cas9 protein and nucleic acids are highly nonlinear, the linear regression model cannot capture the essence of CRISPR-based transcription regulation. As shown in our results, a machine-learning method could overcome

this issue and capture the nonlinearity of the model. Not only did we achieve high accuracy when predicting the regulatory effects of CRISPR-based transcription regulator, but we also demonstrated that this method was not specific to a few selected genes and could be generally applicable. Future work will determine if the results obtained from yeast could provide useful lessons in other eukaryotic systems such as mammalian cells.

We expect that our method will provide a valuable tool for metabolic engineering, especially yeast metabolic engineering at this stage. *S. cerevisiae* is a widely used industrial workhorse for producing a broad spectrum of chemicals that represents over quarter trillion dollars market<sup>38</sup>. The experimental and analytical approaches described here raise the possibility of genome-scale reprogramming of metabolic fluxes, which will dramatically speed up the “design-build-test” cycle in industrial biomanufacturing<sup>39</sup>. We also expect our method could be used to rewire the fate of yeast cells, such as cell cycle, and thus generate new biological insights on the fundamentals of metabolic diseases, aging and apoptosis by using yeast as a disease model.

## Methods

**Strain and plasmid construction in *Saccharomyces cerevisiae*.** dCas9 was codon-optimized for expression in *S. cerevisiae* and cloned into a pRS413 backbone under control of the GAL1 promoter. The RNA-guided transcription factors were built by fusing four repeats of the minimal domain of the herpes simplex viral protein 16 (VP16) to the C-terminus of dCas9 (dCas9\_VP64)<sup>18</sup>. The reporter genes eGFP under the control of the

TEF1p promoter, sapphire under PDC1p, mCherry under TPI1p, and venus under PGK1p were cloned into pRS416 plasmid by using the DNA assembler method<sup>40, 41</sup>. The reporter plasmid for verification was built by cloning tdTomato under the control of ENO2p into pRS416 plasmid. To build gRNA-expressing plasmids, empty gRNA expressing vectors were first made by cloning the pRPR1 promoter (an RNA-polymerase-III-dependent promoter), the gRNA handle (flanked by HindIII and Xho1 sites), and the RPR1 terminator into the SacI and KpnI sites of the pRS425 plasmid. Sequences of the constructs that were used in this study were listed in Table S1. Strains constructed in this study were listed in Table S2.

**Fluorescence Assays.** To assess expression of the reporter constructs, yeast cells expressing different gRNAs (or no gRNA as control) were grown overnight (250 rpm, 30°C) in 3 mL SC medium supplemented with glucose with appropriate selection (three independent cultures for each sample). Ten microliters of these cultures were then transferred into fresh media, supplemented with galactose and grown for 20 h (250 rpm, 30°C) before analysis by plate reader. The wave lengths of the different reporter genes are eGFP:  $\lambda_{\text{ex}}$  488 nm,  $\lambda_{\text{em}}$  507nm; Sapphire:  $\lambda_{\text{ex}}$  399 nm,  $\lambda_{\text{em}}$  511nm; Venus  $\lambda_{\text{ex}}$  515 nm,  $\lambda_{\text{em}}$  528nm; tdTomato  $\lambda_{\text{ex}}$  554 nm,  $\lambda_{\text{em}}$  581nm; mCherry  $\lambda_{\text{ex}}$  587 nm,  $\lambda_{\text{em}}$  610 nm. All of the fold-changes of the synthetic genetic cassettes, including the four cassettes for model training and the ENO2p-tdTomato cassette for model validation, were listed in Table S3 and Table S4.

**Qualitative analysis of key parameters.** The exponential fold changes of different

gRNA designs have been separated into two categories, the promoter region (location < 0, n = 52) and the gene coding region (location > 0, n = 86). The unpaired two-tail t-test was used to calculate the significance of the fold changes between these two groups. For the analysis of the PAM type, the same t-test was used for each PAM types ( $n_{\text{AGG}} = 42$ ,  $n_{\text{TGG}} = 69$ ,  $n_{\text{CGG}} = 21$ ,  $n_{\text{GGG}} = 6$ ).

**Modeling.** The multiple linear regression model was implemented by the “*regress*” command in MATLAB. To evaluate the prediction power, the ten-fold cross validation was implemented for the linear model. The Pearson’s correlation coefficient between observed and predicted fold changes was calculated by MATLAB. The binary regression decision tree model was developed by using “*fittree*” command in MATLAB with all the default setting of options. The details of the decision tree model were shown in Table S5. The ten-fold cross validation was implemented for this model with the same manner. A detailed tutorial of CRISTINES was included in the supplementary information.

**Ten-fold cross validation.** All the datasets from the four synthetic genetic cassettes (n = 151) were randomly divided into ten folds (nine folds with 15 datasets each and one-fold with 16 datasets). Nine of the ten folds were used as training datasets, and the one-fold remaining was used as validation datasets. By iteratively repeating the above process for ten times, all the folds could be used as validation datasets. The Pearson’s correlation coefficient between the observed fold changes and predicted fold changes were calculated by MATLAB.

**Analysis of products from violacein pathway.** Yeast strains for violacein biosynthesis were constructed and product distributions were analyzed as described previously with minor modifications. The parent yeast strain for these experiments was BY4741. The five-gene cassette of violacein pathway was constructed using the DNA assembler method: VioA under TEF1p; VioB under PGK1p; VioC under ENO2p; VioD under TPI1p and VioE under PDC1p. Yeast strains with violacein pathway genes and the CRISPR system with constitutive dCas9 expression were grown in SC medium containing 5% galactose. After 3 days at 30 °C, approximately 2 mL of yeast cultures were harvested and the cells were collected and suspended in 250 µL of methanol, boiled at 95 °C for 15 minutes, and vortexed twice during the incubation. Solutions were centrifuged twice to remove cell debris, and the products from violacein pathway (i.e., violacein, proviolacein, deoxyviolacein, and prodeoxyviolacein) in the supernatant were analyzed by HPLC on an Agilent Rapid Resolution SB-C18 column as described previously, measuring absorbance at 565 nm<sup>42</sup>.

**Code availability.** We claim that the code mentioned in this study is available within the article's Supplementary Information files (Supplementary Software) and at <https://sites.google.com/a/vt.edu/biomolecular-engineering-lab/> as a MATLAB package file (MathWorks Inc.).

**Data availability.** All data generated or analyzed during this study are included in this published article and its Supplementary Information files.

## Acknowledgement

We thank the Writing Center in Virginia Tech for improving the language of the paper. This study was supported by start-up fund (#175323) and the ICTAS Junior Faculty Award from Virginia Tech.

## Author contributions

X.F. contributed to the initial idea of this project. J.S., C.A., and B.F. contributed to the molecular biology experiments and data screening. W.G. and X.F. contributed to the computational modeling and analysis. J.S. and W.G. contributed to the experimental validation and violacein pathway showcase. W.G. and M.P. contributed to the offline software development. J.S., W.G., and X.F. contributed to the manuscript preparation and revision.

## Competing financial interests.

The authors do not have any conflicts of financial interests.

## Supplementary Information

**Figure S1.** The OD<sub>600</sub> fold change for all the strains used for screening. (A) OD<sub>600</sub> fold-change for GFP screening set. (B) OD<sub>600</sub> fold-change for Sapphire screening set. (C) OD<sub>600</sub> fold-change for mCherry screening set. (D) OD<sub>600</sub> fold-change for Venus screening set. The results showed that no significant metabolic burden could be detected compared with wild type strain. The strains marked with (\*) indicated a significant inhibition of growth ( $p < 0.05$ ).

**Figure S2.** Linear model for predicting transcriptional regulation by dCas9-VP64. (A) Pearson's correlation coefficients between each guide RNA design parameters and the fold changes of gene expressions from the screening

data of the four synthetic genetic cassettes. (B) Simulation accuracy of the linear model. (C) Validation of the linear model by comparing the simulated and experimentally measured gene regulations on Eno2p-tdTomato cassette subject to dCas9-VP64 regulation.

**Figure S3.** Screenshot of CRISTINES software with a demo sequence.

**Table S1.** DNA sequences and plasmids used in this study.

**Table S2.** Strains used in this study.

**Table S3.** Key parameters of guide RNAs used in this study.

**Table S4.** Key parameters of guide RNAs used in validation experiments (Eno2p-tdTomato).

**Table S5.** Binary regression decision tree model.

**Table S6.** Measured and predicted concentrations of products from violacein pathway

**Supplementary Software.** CRISTINES toolbox.

## References

1. Lee, S.K., Chou, H., Ham, T.S., Lee, T.S. & Keasling, J.D. Metabolic engineering of microorganisms for biofuels production: from bugs to synthetic biology to fuels. *Current Opinion in Biotechnology* **19**, 556-563 (2008).
2. Keasling, J.D. & Chou, H. Metabolic engineering delivers next-generation biofuels. *Nature biotechnology* **26**, 298-299 (2008).
3. Vuoristo, K.S., Mars, A.E., Sanders, J.P., Eggink, G. & Weusthuis, R.A. Metabolic Engineering of TCA Cycle for Production of Chemicals. *Trends Biotechnol* **34**, 191-197 (2016).
4. Chen, X. et al. Metabolic engineering of *Escherichia coli*: a sustainable industrial platform for bio-based chemical production. *Biotechnology advances* **31**, 1200-1223 (2013).
5. Yadav, V.G. & Stephanopoulos, G. Metabolic Engineering: The Ultimate Paradigm for Continuous Pharmaceutical Manufacturing. *ChemSusChem* **7**, 1847-1853 (2014).
6. Khosla, C. & Keasling, J.D. Metabolic engineering for drug discovery and development. *Nature reviews. Drug discovery* **2**, 1019-1025 (2003).
7. Keasling, J.D. Manufacturing Molecules Through Metabolic Engineering. *Science* **330**, 1355-1358 (2010).
8. Zadran, S. & Levine, R.D. Perspectives in metabolic engineering: understanding cellular regulation towards the control of metabolic routes. *Appl Biochem Biotechnol* **169**, 55-65 (2013).
9. Zalatan, J.G. et al. Engineering complex synthetic transcriptional programs with CRISPR RNA scaffolds. *Cell* **160**, 339-350 (2015).
10. McNerney, M.P., Watstein, D.M. & Styczynski, M.P. Precision metabolic engineering: The design of responsive, selective, and controllable metabolic systems. *Metabolic engineering* **31**, 123-131 (2015).
11. Broun, P. Transcription factors as tools for metabolic engineering in plants. *Curr Opin Plant Biol* **7**, 202-209 (2004).
12. Kim, J. & Reed, J.L. OptORF: Optimal metabolic and regulatory perturbations for metabolic engineering of microbial strains. *BMC Syst Biol* **4**, 53 (2010).
13. Cong, L. et al. Multiplex genome engineering using CRISPR/Cas systems. *Science* **339**, 819-823 (2013).
14. Jiang, W., Bikard, D., Cox, D., Zhang, F. & Marraffini, L.A. RNA-guided editing of bacterial genomes using CRISPR-Cas systems. *Nature biotechnology* **31**, 233-239 (2013).
15. Gilbert, L.A. et al. CRISPR-mediated modular RNA-guided regulation of

- transcription in eukaryotes. *Cell* **154**, 442-451 (2013).
16. Larson, M.H. et al. CRISPR interference (CRISPRi) for sequence-specific control of gene expression. *Nature protocols* **8**, 2180-2196 (2013).
  17. Qi, L.S. et al. Repurposing CRISPR as an RNA-guided platform for sequence-specific control of gene expression. *Cell* **152**, 1173-1183 (2013).
  18. Farzadfar, F., Perli, S.D. & Lu, T.K. Tunable and multifunctional eukaryotic transcription factors based on CRISPR/Cas. *ACS Synth Biol* **2**, 604-613 (2013).
  19. Bikard, D. et al. Programmable repression and activation of bacterial gene expression using an engineered CRISPR-Cas system. *Nucleic acids research* **41**, 7429-7437 (2013).
  20. Gao, Y. et al. Complex transcriptional modulation with orthogonal and inducible dCas9 regulators. *Nature methods* **13**, 1043-1049 (2016).
  21. Montague, T.G., Cruz, J.M., Gagnon, J.A., Church, G.M. & Valen, E. CHOPCHOP: a CRISPR/Cas9 and TALEN web tool for genome editing. *Nucleic acids research* **42**, W401-W407 (2014).
  22. Labun, K., Montague, T.G., Gagnon, J.A., Thyme, S.B. & Valen, E. CHOPCHOP v2: a web tool for the next generation of CRISPR genome engineering. *Nucleic acids research* **44**, W272-W276 (2016).
  23. Russell, S.J. & Norvig, P. Artificial Intelligence: A Modern Approach. (Pearson Education, 2003).
  24. Langley, P. The changing science of machine learning. *Machine Learning* **82**, 275-279 (2011).
  25. Mohri, M., Rostamizadeh, A. & Talwalkar, A. Foundations of machine learning. (MIT press, 2012).
  26. Breiman, L., Friedman, J., Stone, C.J. & Olshen, R.A. Classification and regression trees. (CRC press, 1984).
  27. Loh, W.-Y. & Shih, Y.-S. Split selection methods for classification trees. *Statistica sinica*, 815-840 (1997).
  28. Hoshino, T. Violacein and related tryptophan metabolites produced by *Chromobacterium violaceum*: biosynthetic mechanism and pathway for construction of violacein core. *Applied microbiology and biotechnology* **91**, 1463-1475 (2011).
  29. Cho, S.W. et al. Analysis of off-target effects of CRISPR/Cas-derived RNA-guided endonucleases and nickases. *Genome research* **24**, 132-141 (2014).
  30. Haeussler, M. et al. Evaluation of off-target and on-target scoring algorithms and integration into the guide RNA selection tool CRISPOR. *Genome biology* **17**, 148 (2016).
  31. Delebecque, C.J., Lindner, A.B., Silver, P.A. & Aldaye, F.A. Organization of intracellular reactions with rationally designed RNA assemblies. *Science* **333**, 470-474 (2011).
  32. Farasat, I. & Salis, H.M. A Biophysical Model of CRISPR/Cas9 Activity for Rational Design of Genome Editing and Gene Regulation. *PLoS Comput Biol* **12**, e1004724 (2016).
  33. Nishimasu, H. et al. Crystal structure of Cas9 in complex with guide RNA and target DNA. *Cell* **156**, 935-949 (2014).
  34. Jinek, M. et al. Structures of Cas9 endonucleases reveal RNA-mediated conformational activation. *Science* **343**, 1247997 (2014).
  35. Slaymaker, I.M. et al. Rationally engineered Cas9 nucleases with improved specificity. *Science* **351**, 84-88 (2016).
  36. Jiang, F. et al. Structures of a CRISPR-Cas9 R-loop complex primed for DNA cleavage. *Science* **351**, 867-871 (2016).
  37. Jiang, F., Zhou, K., Ma, L., Gressel, S. & Doudna, J.A. STRUCTURAL BIOLOGY. A Cas9-guide RNA complex preorganized for target DNA recognition. *Science* **348**, 1477-1481 (2015).

38. Hittinger, C.T. *Saccharomyces* diversity and evolution: a budding model genus. *Trends in genetics : TIG* **29**, 309-317 (2013).
39. Petzold, C.J., Chan, L.J.G., Nhan, M. & Adams, P.D. Analytics for Metabolic Engineering. *Frontiers in Bioengineering and Biotechnology* **3**, 135 (2015).
40. Shao, Z., Zhao, H. & Zhao, H. DNA assembler, an *in vivo* genetic method for rapid construction of biochemical pathways. *Nucleic acids research* **27**, e16 (2009).
41. Shao, Z., Luo, Y. & Zhao, H. Rapid characterization and engineering of natural product biosynthetic pathways via DNA assembler. *Mol Biosyst* **7**, 1056-1059 (2011).
42. Lee, M.E., Aswani, A., Han, A.S., Tomlin, C.J. & Dueber, J.E. Expression-level optimization of a multi-enzyme pathway in the absence of a high-throughput assay. *Nucleic acids research* **41**, 10668-10678 (2013).

## **Supplementary method**

### **1. Binary regression decision tree model**

#### **1.1. Parameterization of guide RNAs**

Nine key design parameters, i.e., location, GC content (GC%), minimal free energy ( $\Delta G$ ), number of base A, number of base G, AGG, TGG, CGG, and GGG, have been extracted from guide RNAs, respectively. Location is defined as the number of bases between the first base of guide RNA binding sequence and the A in the start codon (ATG). Therefore, the position of A in the ATG is considered as 0. The location of guide RNAs binding before the start codon is defined as negative, and vice versa. The GC content (GC%) is defined as the proportion of base G and base C in the guide RNA sequence. Minimal free energy ( $\Delta G$ ) is calculated by *rnafold* command in MATLAB. As a categorical parameter, AGG, TGG, CGG, and GGG are four bool parameters representing four types of the PAM site type. Each guide RNA has a set of key design parameters. The parameters are used to train and validate the decision tree model.

#### **1.2. Setup of regression decision tree model**

To train the binary regression decision tree model, “*fittree*” command in MATLAB was used with the default settings. In detail, the standard CART algorithm was used to select the best split predictor, which maximized the split-criterion gain over all possible splits of all predictors. The “*fittree*” grew the regression tree and estimated the optimal sequence of pruned subtrees based on the equally weighted mean squared errors, but did not prune the regression tree. During the tree growing, splitting nodes stopped when quadratic error per node dropped below  $10^{-6}$  of the quadratic error for the entire data computed before the decision tree was grown. To control the depth of the tree and avoid the over-fitting of the tree model, the maximum splits number was the number of guide RNAs in training datasets.

#### **1.3. Application of regression decision tree model**

To apply our binary regression decision tree model, “*predict*” command in MATLAB was used to predict the fold changes of gene expression levels for specific guide RNAs. ([https://www.mathworks.com/help/stats/compactregressiontree.predict.html?searchHighlight=pr edict&s\\_tid=doc\\_srchtitle](https://www.mathworks.com/help/stats/compactregressiontree.predict.html?searchHighlight=pr edict&s_tid=doc_srchtitle)). In general, the target guide RNA sequence will be first processed by customized functions (supplementary software) to calculate the corresponding design parameters. An input matrix will be generated for the tree model, which will be used to predict the corresponding fold change of the gene expression level.

#### **1.4 CRISTINES software and its results**

CRISTINES software is an offline MATLAB-based tool to provide the guide RNA designs to achieve gene up-regulation and down-regulation. The core algorithm is the binary regression decision tree model that uses the key design parameters of guide RNAs as the input. In the CRISTINES, the sequence of interest with the identification of the start codon ATG, is used as the source file. All the possible guide RNAs from the input sequence will be generated, and the nine design parameters, i.e., location, GC content, minimal free energy, number of base A,

number of base G, AGG, TGG, CGG, and GGG, are calculated for each of guide RNAs. These design parameters will then be used in the binary regression decision tree model to calculate the regulatory effects (i.e., fold change of gene expression level) of guide RNAs. CRISTINES will report the top 5 guide RNA designs with highest up- and down- regulation effects, respectively. The regulatory effects of all possible guide RNAs can be downloaded to the local folder in Excel file.

## **2. Calculation of metabolic fluxes in violacein pathway subject to dCas9-VP64 regulation**

We hypothesized that the changes gene expression levels would quantitatively change the metabolic fluxes in the branches of violacein pathway, and thus, leading to different concentrations of various products. In detail, the flows through pathways governed by gene *vioA*, *vioB*, *vioC*, *vioD*, and *vioE*, are defined as  $f_A$ ,  $f_B$ ,  $f_C$ ,  $f_D$ , and  $f_E$ , respectively. The predicted fold changes of gene *vioA*, *vioB*, *vioC*, *vioD*, and *vioE*, are defined as  $FC_A$ ,  $FC_B$ ,  $FC_C$ ,  $FC_D$ , and  $FC_E$ , respectively. Similarly, the flows through the non-enzymatic pathways for producing the final colorful chemical, proviolacein, prodeoxyviolacein, violacein, and deoxyviolacein, are defined as  $f_{PV}$ ,  $f_{PDV}$ ,  $f_V$ , and  $f_{DV}$ , respectively. To calculate the effects of dCas9-VP64 on metabolic fluxes in violacein pathway, we assume a pseudo-steady state was achieved. Thus, based on the flux balance at steady state, the quantitative relations among these parameters were shown below:

$$f_A = f_B = f_E \quad \text{Eq. 1}$$

$$f_E = f_{DV} + f_{PDV} + f_D \quad \text{Eq. 2}$$

$$f_D = f_V + f_{PV} \quad \text{Eq. 3}$$

$$f_C = f_{DV} + f_V \quad \text{Eq. 4}$$

In addition, we hypothesized that the proportion between  $f_{DV}$  and  $f_V$  obeys the Hill equation as shown in Eq. 5 with Hill coefficient defined as  $n$ :

$$f_{DV} / f_V = 1 / (f_C^n + 1) \quad \text{Eq. 5}$$

The values of  $f_{PV}$ ,  $f_{PDV}$ ,  $f_V$ , and  $f_{DV}$  can be directly obtained from the HPLC measurements, which would serve as the experimental measurements. The constant  $n$  was calculated as 0.356 from the measurements of the control strain by using Eq. 4 and Eq. 5. The following methods were used to calculate the simulated  $f_{PV}$ ,  $f_{PDV}$ ,  $f_V$ , and  $f_{DV}$ .

- 1) If the dCas9-VP64 system regulates the gene expression of *vioA* or *vioE*, then  $f_E = FC_A * f_{E, \text{Control}}$  or  $f_E = FC_E * f_{E, \text{Control}}$ , respectively;  $f_D = FC_D * f_{D, \text{Control}}$ , and  $f_C = FC_C * f_{C, \text{Control}}$ .
- 2) If the dCas9-VP64 system regulates the gene expression of *vioC*, then  $f_C = FC_C * f_{C, \text{Control}}$ ,  $f_E = f_{E, \text{Control}}$ , and  $f_D = f_{D, \text{Control}}$ .
- 3) If the dCas9-VP64 system regulates the gene expression of *vioD*, then  $f_D = FC_D * f_{D, \text{Control}}$ ,  $f_E = f_{E, \text{Control}}$ , and  $f_C = f_{C, \text{Control}}$ .
- 4) If the dCas9-VP64 system is regulating multiple gene expression in the violacein pathways, we assume that the regulation of each gene is independent to others. In other

words, we hypothesized that the regulation of dCas9-VP64 system was independent on each gene and each pathway of the violacein pathways.

By knowing  $f_E$ ,  $f_D$ , and  $f_C$ , we could then solve Eq 1-5 together to derive the simulated  $f_{DV}$ ,  $f_V$ ,  $f_{PV}$ , and  $f_{PDV}$  sequentially. We next compared the experimentally measured and simulated  $f_{DV}$ ,  $f_V$ ,  $f_{PV}$ , and  $f_{PDV}$  as shown in Fig. 3B and 3C.

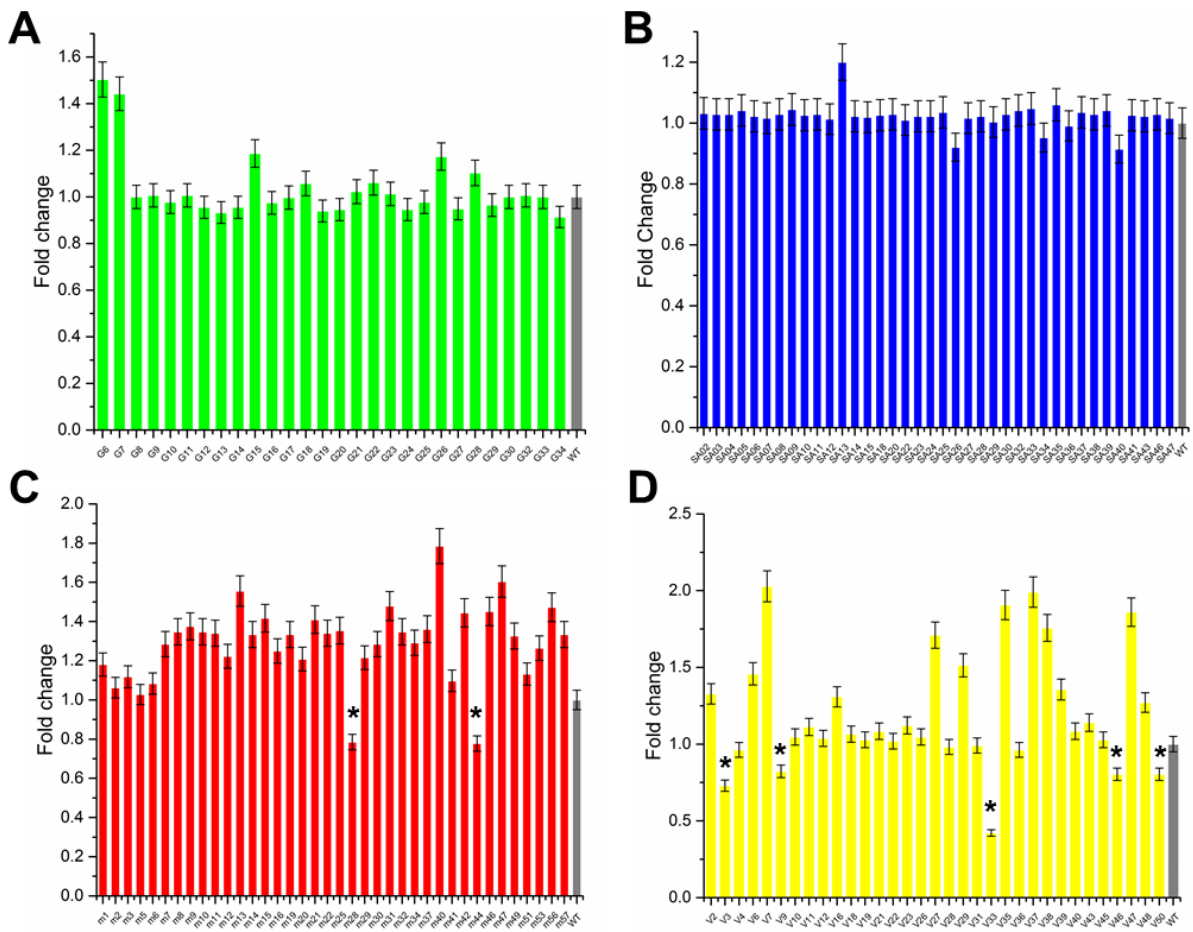


**Figure S1.** The OD<sub>600</sub> fold change for all the strains used for screening. (A) OD<sub>600</sub> fold-change for GFP screening set. (B) OD<sub>600</sub> fold-change for Sapphire screening set. (C) OD<sub>600</sub> fold-change for mCherry screening set. (D) OD<sub>600</sub> fold-change for Venus screening set. The results showed that no significant metabolic burden could be detected compared with wild type strain. The strains marked with (\*) indicated a significant inhibition of growth ( $p < 0.05$ ).

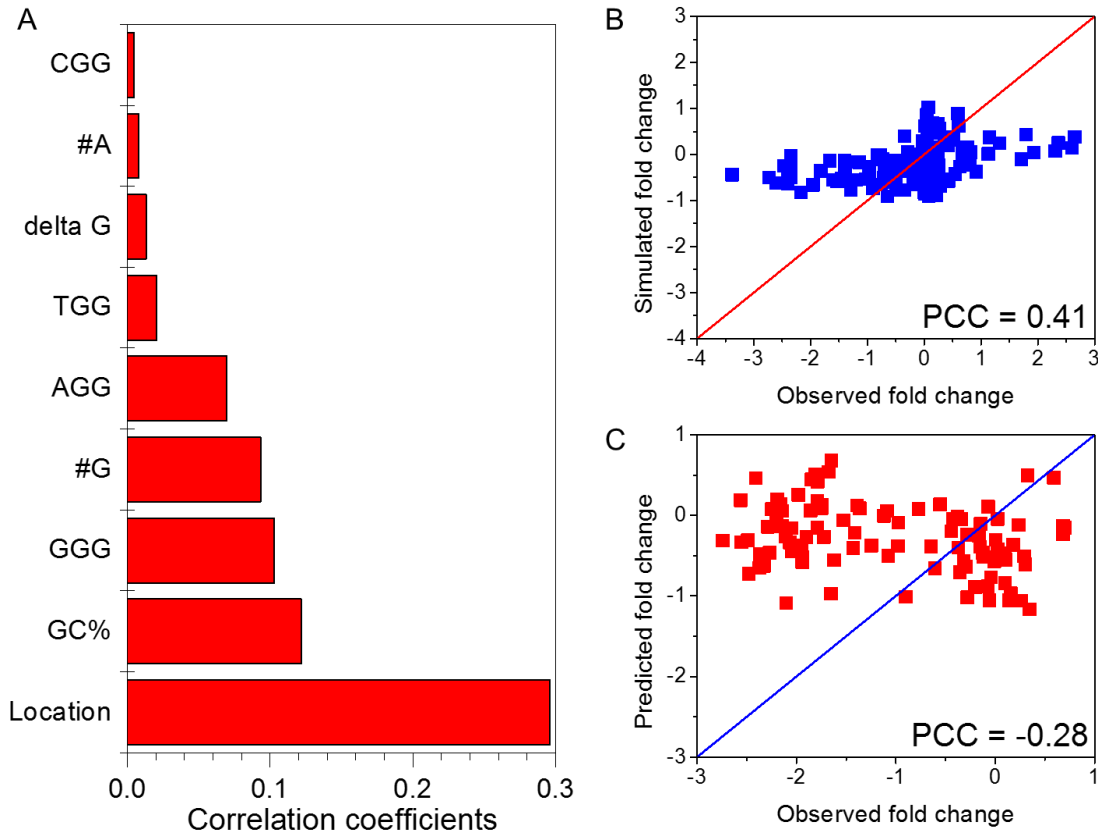


**Figure S2.** Linear model for predicting transcriptional regulation by dCas9-VP64. (A) Pearson's correlation coefficients between each guide RNA design parameters and the fold changes of gene expressions from the screening data of the four synthetic genetic cassettes. (B) Simulation accuracy of the linear model. (C) Validation of the linear model by comparing the simulated and experimentally measured gene regulations on Eno2p-tdTomato cassette subject to dCas9-VP64 regulation.

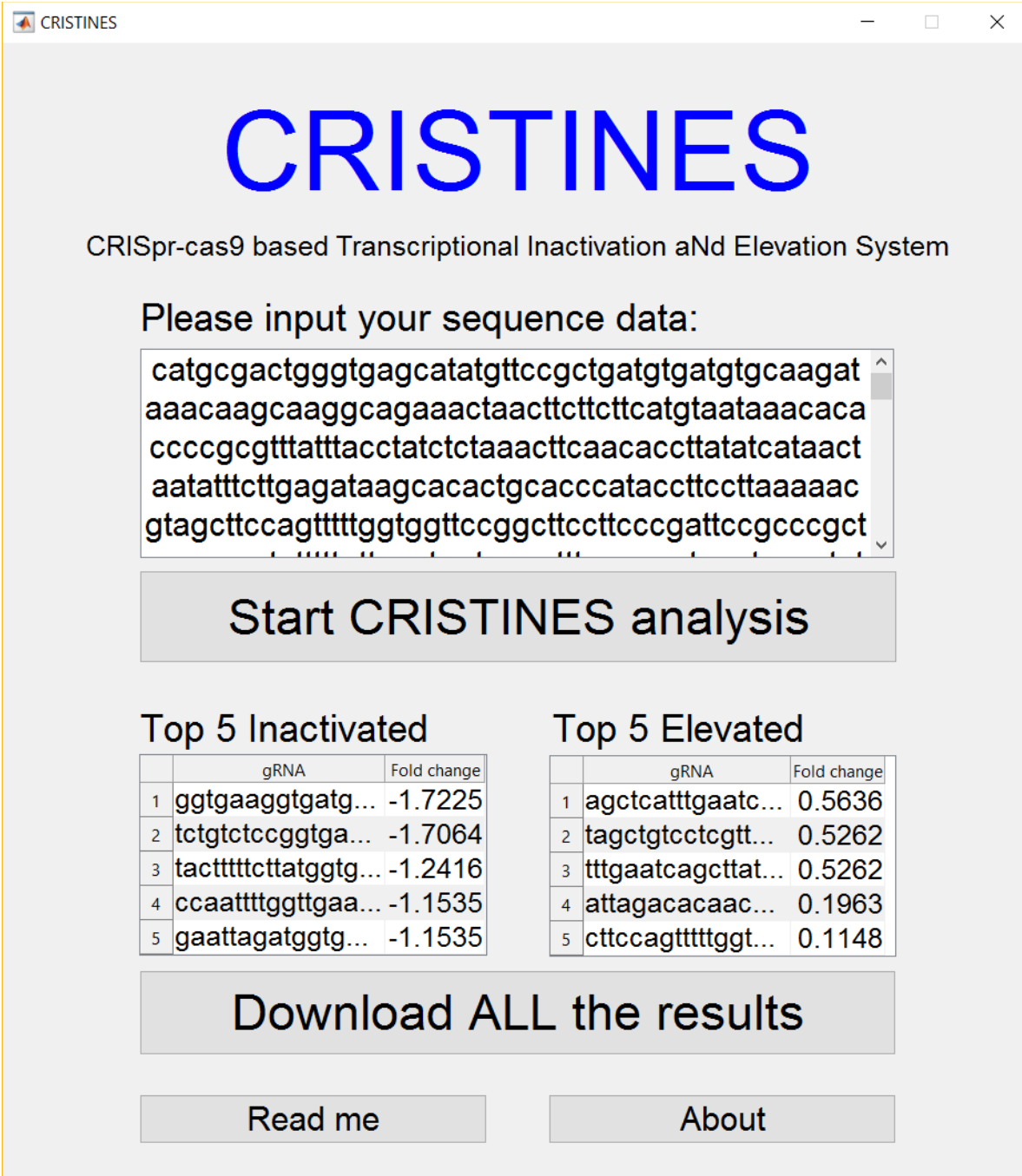


**Figure S3.** Screenshot of CRISTINES software with a demo sequence.

**Table S1.** DNA sequences and plasmids used in this study.







\* All the gRNAs use the same structure except the 20bp targeting to different sites.

**Table S2.** Strains used in this study.

Name	Phenotype	Plasmids
TEF1p(H)	INVSc1: MATa his3D1 leu2 trp1-289 ura3-52 MAT his3D1 leu2 trp1-289 ura3-52	pViolacein, pCas9, pgRNA-TEF1p(H)
TEF1p(M)	Same as INVSc1	pViolacein, pCas9, pgRNATEF1p(M)
TEF1p(L)	Same as INVSc1	pViolacein, pCas9, pgRNATEF1p(L)
PDC1p(H)	Same as INVSc1	pViolacein, pCas9, pgRNAPDC1p(H)
PDC1p(M)	Same as INVSc1	pViolacein, pCas9, pgRNAPDC1p(M)
PDC1p(L)	Same as INVSc1	pViolacein, pCas9, pgRNAPDC1p(L)
TPI1p(M)	Same as INVSc1	pViolacein, pCas9, pgRNATPI1p(M)
TPI1p(L)	Same as INVSc1	pViolacein, pCas9, pgRNATPI1p(L)
ENO2p(H)	Same as INVSc1	pViolacein, pCas9, pgRNAENO2p(H)
ENO2p(M)	Same as INVSc1	pViolacein, pCas9, pgRNAENO2p(M)
ENO2p(L)	Same as INVSc1	pViolacein, pCas9, pgRNAENO2p(L)
ACD	Same as INVSc1	pViolacein, pCas9, pgRNATEF1p(H)-gRNAENO2p(H)-gRNATPI1p(L)
CD	Same as INVSc1	pViolacein, pCas9, pgRNAENO2p(H)-gRNATPI1p(L)
AD	Same as INVSc1	pViolacein, pCas9, pgRNATEF1p(H)-gRNATPI1p(L)

**Table S3.** Key parameters of guide RNAs used in this study for model training.

TEF1p-GFP

ATAGCTTCAAAATGTTCTACTCCTTTTACTCTTCAGATTTCTCGGACTCCGCGC  
 ATCGCCGTACCACTCAAAACACCCAAGCACAGCATACTAAATTCCCTCTTC  
 CTCTAGGGTGTGTTAATTACCGTACTAAAGGTTGGAAAAGAAAAAGAGACCGC  
 CTCGTTCTTTCTCGTCAAAAAGGCAATAAAAATTTCACGTTCTTTCT  
G1  
 TGAAAATTGTTTGATTTCTTCGATGACCTCCCATTGATATTAAAGTTA  
 ATAAACGGTCTTCAATTCTCAAGTTCAAGTTCAAGTTCTTCTTGTCTATTACAAC  
G2  
 TTTACTTCTGCTCATTAGAAAGAAAGCATAGCAATCTAAGTTAATTACAAA  
**ATGTCTAAAGGTGAAGAATTATTCACTGGTGTGTC**CCAATTTGGTGAATTAGATG  
G3 G4 G5 G6  
 GTGATGTTAATTGGTCACAAATTCTGTCTCCGGTGAAGGTGAAGGTGATGCTACTTA  
G7 G8 G9 G10  
CGGTAAATTGACCTTAAATTATTGTACTACTTGGTAAATTGCCAGTCCATGGCCAA  
G11 G12 G13  
 CCTTAGTCACTACTTAACCTATGGTGTCAATGTTTCTAGATACCCAGATCATATGA  
G14  
 AACAAACATGACTTTCAAGTCTGCCATGCCAGAAGGTTATGTTCAAGAAAGAACTAT  
G15  
 TTTTTCAAAGATGACGGTAACTACAAGACCAGAGCTGAAGTCAAGTTGAAGGTGA  
G16 G17  
 TACCTTAGTTAATAGAACATCGAATTAAAAGGTATTGATTAAAGAAGATTGGTAAACATT  
G18 G19  
TAGGTCACAAATTGGAATACAACTATAACTCTCACAAATGTTACATCATGGCTGACAA  
G20 G21 G22  
 ACAAAAGAATGGTATCAAAGTTAACTCAAAATTAGACACAAACATTGAAGATGGTTCT  
G23 G24  
 GTTCAATTAGCTGACCATTATCAACAAACTCCAATTGGTGATGGCCAGTCTGTT  
G25  
 ACCAGACAACCATTACTTATCCACTCAATCTGCCTATCCAAAGATCCAAACGAAAAG  
 AGAGACCACATTGGTCTTGTAGAATTGTTACTGCTGCTTGGTATTACCCATGGTATGGA  
G26 G27 G28  
 TGAATTGTACAAA

No.	Location	GC%	ΔG	AGG	TGG	CGG	GGG	#G	#A	Fold change (log2)
G1	-213	0.3	-9.1	1	0	0	0	2	4	0.00
G2	-114	0.1	-7.3	0	0	1	0	2	9	-0.02
G3	9	0.15	-9.3	1	0	0	0	1	9	-3.38
G4	27	0.3	-12	0	1	0	0	4	9	-0.29

G5	44	0.45	-11	0	1	0	0	4	3	0.01
G6	57	0.3	-7.8	0	1	0	0	4	6	0.07
G7	69	0.3	-7	0	1	0	0	6	7	0.03
G8	90	0.4	-8.4	0	0	1	0	3	4	-0.24
G9	96	0.4	-9.5	1	0	0	0	4	4	-0.50
G10	102	0.55	-10.8	1	0	0	0	7	3	-1.54
G11	117	0.45	-8.8	0	0	1	0	7	5	-0.09
G12	150	0.15	-10.4	0	1	0	0	1	7	-0.15
G13	169	0.45	-12.9	0	1	0	0	4	5	-0.24
G14	198	0.25	-8.6	0	1	0	0	1	6	0.07
G15	270	0.5	-9.9	1	0	0	0	4	5	-0.01
G16	309	0.2	-8	0	0	1	0	2	7	-0.19
G17	345	0.4	-10	1	0	0	0	6	7	-0.35
G18	378	0.2	-7.1	1	0	0	0	3	10	-0.04
G19	399	0.25	-7.9	0	1	0	0	5	8	0.05
G20	411	0.25	-10.8	1	0	0	0	4	9	0.08
G21	422	0.25	-8.1	0	1	0	0	2	8	-0.97
G22	458	0.35	-7.1	0	1	0	0	1	6	0.08
G23	477	0.35	-7.6	0	1	0	0	4	11	-0.31
G24	519	0.3	-7	0	1	0	0	3	10	0.13
G25	564	0.25	-8.1	0	1	0	0	0	10	-0.21
G26	653	0.4	-7	0	1	0	0	4	12	-0.12
G27	681	0.35	-8.9	0	1	0	0	4	4	0.00
G28	693	0.5	-14.5	0	1	0	0	4	4	0.21

### TPI1p-mCherry

TATATCTAGGAACCCATCAGGT**TGGTGG**AAGATTACCCGTTCAAGACTTTCAGCTTC  
                                   M1  M2

CTCTATTGATGTTACACCT**TGG**ACACCCCTTTCTGGCATCCAGTTTAATCTTCAG**TG**  
                                   M3  M4

**GC**ATGTGAGATTCTCCGAAATTAAATTAAAGCAATCACACAATTCT**CGG**ATACCACCT  
   M5

**CGG**TTGAAACTGAC**AGGTGG**TTTGTACGCATGCTAATGCAA**AGGAGCCTATA**ACCT  
   M6                          M7  M8  M9

**TGG**CT**CGG**CTGCTGTAAC**AGG**GAATATAA**AGG**GCAGCATAATT**AGG**AGTTAGTGA  
   M10  M11                  M12                          M13                  M14

ACTTGCAACATTACTATTTCCTCTTACGTAAATATTTCCTTTAATTCTAAATCA

ATCTTTCAATTGGTTGTATTCTTCTTGCTTAAATCTATAACTACAAAAAACAA

CATAACATAAA**TGG**TTAGCAAAGGCGAGGAAGATAACA**TGG**CTATAATCAA  
                                   M15  M16

AGAGTTATGAGATTCAAAGTACACA**TGGAGG**GTTCACTGAAT**TGG**CATGAATTGAA  
                                   M17  M18                                  M19

ATTGAAGGCGAAGGCG**AGG**GCAGACCTTACGAAGGAACCAAACAGCAAAACTAA  
                                   M20

GGTAACAAAAGGTGGTCCTCTGCCATCGCCTGGGACATTCTCAGTCCACAATTGATG  
M21 M22 M23  
TA CGGTTCTAAAGCGTACGTCAAACATCCAGCAGACATTCCAGATTACTTGAAATTG  
M24  
CTTTCCAGA AGG CTTTAAGTGGGAAAGAGTTATGAACCTCGAGGATGGA GGGGTTG  
M25 M26 M27  
TGACCGTTACGCAAGATTCCCTTTACAAGATGGTGAGTTATCTACA AGGTCAAATT  
M28  
AAGGGGGACTAATTCCTTCAGACGGGCCAGTCATGCAGAAAAAGACTATGGGATG  
M29 M30 M31 M32  
GGAAGCCTCTCAGAGAGAATGTATCCTGAAGATGGCGCTCTAAAAGGAGAAATCAA  
M33  
GCAAAGATTGAAGTAAAGGACGGAGGTTCATTATGATGCAGAAGTAAAAACAAACCTA  
M34 M35  
TAAAGCTAAAAGCCAGTTCAACTTCCTGGTGCCCTACAATGTTAACATCAAGCTAGAC  
ATTACATCCCATAATGAAGATTACACTATAGTGGAACAGTATGAACGTGCTGAAGGTA  
M36  
GACACAGTACAGGTGGTATGGATGAACGTACAAG  
M37 M38

No.	Location	GC%	Energy	AGG	TGG	CGG	GGG	#G	#A	Fold change (log2)
M1	-408	0.45	-11.8	0	1	0	0	4	6	2.36
M2	-405	0.55	-14.5	0	1	0	0	6	5	2.31
M3	-353	0.4	-8.2	0	1	0	0	2	4	2.65
M4	-314	0.3	-7.4	0	1	0	0	2	5	2.60
M5	-265	0.35	-8.2	0	0	1	0	1	8	1.79
M6	-253	0.45	-8.6	0	0	1	0	2	5	1.15
M7	-239	0.55	-10.7	1	0	0	0	4	5	0.35
M8	-236	0.55	-10.5	0	1	0	0	6	5	0.76
M9	-211	0.4	-11.4	1	0	0	0	4	6	0.81
M10	-194	0.4	-14.2	0	1	0	0	3	7	1.93
M11	-189	0.45	-12.2	0	0	1	0	4	4	0.10
M12	-176	0.55	-11.1	1	0	0	0	6	2	0.20
M13	-165	0.35	-7.4	1	0	0	0	5	8	0.26
M14	-150	0.3	-9.6	1	0	0	0	4	8	0.92
M15	2	0.2	-7	0	1	0	0	0	13	0.05
M16	29	0.45	-7	0	1	0	0	6	10	0.22
M17	68	0.3	-7	0	1	0	0	3	9	-0.29
M18	71	0.4	-7.5	1	0	0	0	5	8	0.15
M19	84	0.5	-7.7	0	1	0	0	7	6	-1.14
M20	116	0.5	-10.7	1	0	0	0	8	7	-0.17
M21	165	0.3	-7.2	1	0	0	0	3	11	-0.02
M22	168	0.3	-8.7	0	1	0	0	4	11	0.08
M23	187	0.65	-10.8	0	1	0	0	5	1	0.68
M24	216	0.4	-7	0	0	1	0	2	6	0.67

M25	282	0.3	-8.6	1	0	0	0	3	5	0.28
M26	314	0.4	-8.3	1	0	0	0	6	7	0.03
M27	322	0.4	-11.3	0	0	0	1	6	6	-0.05
M28	377	0.35	-10.3	1	0	0	0	5	6	0.22
M29	388	0.25	-7.1	1	0	0	0	2	8	0.17
M30	389	0.25	-7	0	0	0	1	2	9	0.18
M31	411	0.4	-9.9	0	0	1	0	4	5	-0.60
M32	442	0.4	-7.3	0	1	0	0	6	9	-0.07
M33	477	0.4	-7.2	0	1	0	0	6	8	-0.11
M34	518	0.3	-7	1	0	0	0	4	10	0.43
M35	525	0.4	-7.6	1	0	0	0	7	8	0.02
M36	647	0.25	-7.1	0	1	0	0	3	9	0.34
M37	687	0.5	-7.1	0	1	0	0	7	8	0.54
M38	692	0.45	-8.6	0	1	0	0	6	7	0.41

### PDC1p-Sapphire

CATGCGACTGGGTGAGCATATGTTCCGCTGATGTGATGTGCAAGATAAACAAAGCA**AG**  
**S1**  
**G**CAGAAACTAACTTCTTCATGTAATAAACACACACCCCCGCGTTTATTACCTATCTCT  
AAACTTCAACACCTTATATCATAACTAATATTCTTGAGATAAGCACACTGCACCCATA  
CCTTCCTTAAAAACGTAGCTTCCAGTTTT**TGGTGG**TTCCGGCTTCCCTCCGATTCCG  
S2 S3 S4  
CCCGCTAACGCATATTGGTTGCCT**TGGTGG**CATTGCAAAATGCATAACCTATGCAT  
S5 S6  
TTAAAAGATTATGTATGCTCTGACTTTCTGTGATG**AGGCTCGTGG**AAAAAAATG  
S7 S8  
AATAATTATGAATTGAGAACAAATTGGTTGTTAC**CGGT**ATTTACTAT**TGGA**ATAATC  
S9 S10  
AATCAATTG**AGG**ATTTATGCAAATATCGTTGAATATTTCGACCCTTGAGTACTT  
S11  
TTCTTCATAATTGCATAATATTGTCGCTGCCCTTTCTGTTAGA**CGGT**TGTCTTGATC  
S12  
TACTTGCTATCGTTAACACACCACCTTATTCTAATCTACTATTTTTTAGCTCATTGAAT  
CAGCTTA**TGGTGA****TGG**CACATTTCGATAAACCTAGCTGTCCTCGTTGAACATAGGA  
S13 S14  
AAAAAAAATATAAACAAAGGCTTTCACTCTCCTGCAATCAGATT**TGG**TTTGTTC  
S15  
CCTTATTTCATATTCTGTATTCCTTCTCAATTATTATTCTACTCATAACCTC  
ACGCAAAATAACACAGTCAAATCAATCAAATGTCTAAAGGTGAAGAATTATTC**ACTG**  
S16  
**GTGTTGTCCA**ATTGGTTGAATTAGA**TGGT**GATGTTAA**TGG**TCACAAATTTCGTGTC  
S17 S18  
TCCGGTGA**AGGT**GA**AGGT**GATGCTACTTA**CGG**TAAATTGACCTTAAAATTATTGTA  
S19 S20 S21 S22

CTACT**TGGTAAATTGCCAGTCCA****TGGCCAACCTAGTC**ACTACTTTCTTA**TGGTGTT**  
**S23** **S24** **S25**  
 ATGGTTTTGCTAGATACCCAGATCATATGAAACAAACATGACTTTCAAGTCTGCCAT  
  
 GCCAGA**AGG**TTATGTTCAAGAAAGAACTATTTTCAAAGATGA**CGG**TAACACAA  
**S26** **S27**  
 GACCAGAGCTGAAGTCAAGTTGA**AGG**TGATA**CGG**CTTAGTTAACATAGAACATTAAA  
**S28** **S29**  
**GG**TATTGATTAAAGAAGAT**TGG**TAACATT**AGGT**CACAAAT**TGGA**ATACAACATTAA  
**S30** **S31** **S32**  
 CTCTCACAATGTTACATCA**TGG**CTGACAAACAAAAGAA**TGG**TATCAAAGCTAACTTC  
**S33** **S34**  
 AAAATTAGACACAAACATTGAAGA**TGG**TGGTGTCAATTAGCTGACCATTATCAACAAA  
**S35**  
 ATACTCCAAT**TGG**GATGGTCCAGTCTTGTACCAACACCATTACTTATCCATTCAA  
**S36**  
 TCTGCCTTATCCAAAGATCCAAACGAAAAGAGAGACCACATGGTCTGTTAGAATTG  
  
 TTACTGCTGC**TGG**TATTACCC**TGG**TATGGATGAATTGTACAAA  
**S37** **S38**

No.	Location	GC%	Energy	AGG	TGG	CGG	GGG	#G	#A	Fold change (log2)
S1	-745	0.35	-8.4	1	0	0	0	4	10	-0.35
S2	-596	0.35	-10.1	0	1	0	0	3	6	-0.02
S3	-593	0.45	-11.2	0	1	0	0	5	3	-0.29
S4	-587	0.45	-10.7	0	0	1	0	5	1	0.15
S5	-541	0.35	-8.3	0	1	0	0	3	5	0.03
S6	-538	0.45	-10.4	0	1	0	0	5	2	-0.78
S7	-468	0.4	-8.3	1	0	0	0	5	2	-1.39
S8	-461	0.5	-9.6	0	1	0	0	7	2	-1.29
S9	-413	0.25	-11.6	0	0	1	0	4	6	-1.42
S10	-400	0.3	-8.5	0	1	0	0	4	4	-0.40
S11	-381	0.25	-7.1	1	0	0	0	3	9	-0.08
S12	-283	0.45	-9.2	0	0	1	0	3	2	-0.18
S13	-202	0.35	-10.1	0	1	0	0	3	6	1.13
S14	-196	0.35	-10	0	1	0	0	5	5	-0.02
S15	-103	0.4	-9	0	1	0	0	2	5	-0.02
S16	27	0.3	-12	0	1	0	0	4	9	-2.35
S17	57	0.3	-7.8	0	1	0	0	4	6	-2.40
S18	69	0.3	-7	0	1	0	0	6	7	-1.60
S19	90	0.4	-8.4	0	0	1	0	3	4	-1.40
S20	96	0.4	-9.5	1	0	0	0	4	4	-2.35
S21	102	0.55	-10.8	1	0	0	0	7	3	-1.45
S22	117	0.45	-8.8	0	0	1	0	7	5	-2.60
S23	150	0.15	-10.4	0	1	0	0	1	7	-1.45
S24	169	0.45	-12.9	0	1	0	0	4	5	-0.97

S25	198	0.25	-8.2	0	1	0	0	1	4	-0.71
S26	270	0.5	-9.9	1	0	0	0	4	5	-2.47
S27	309	0.2	-8	0	0	1	0	2	7	-0.82
S28	345	0.4	-10	1	0	0	0	6	7	-1.29
S29	378	0.2	-7.1	1	0	0	0	3	10	-0.76
S30	399	0.25	-7.9	0	1	0	0	5	8	-0.40
S31	411	0.25	-10.8	1	0	0	0	4	9	-0.65
S32	422	0.25	-8.1	0	1	0	0	2	8	-0.40
S33	458	0.35	-7.1	0	1	0	0	1	6	-0.82
S34	477	0.35	-7.6	0	1	0	0	4	11	-1.40
S35	519	0.3	-7	0	1	0	0	3	10	-0.06
S36	564	0.25	-8.1	0	1	0	0	0	10	-2.35
S37	681	0.35	-8.9	0	1	0	0	4	4	-2.17
S38	693	0.5	-14.5	0	1	0	0	4	4	-2.40

### PGK1p-Venus

TCAGGCATGAACGCATCACAGACAAAATCTTCTTGACAAACGTACAATTGATCCCTC  
 CCCATCCGTTATCACAATGACAGGTGTCATTTGTGCTCTTAT**TGGG**ACGATCCTTATT  
V1 V2  
 CCGCTTCATC**CGG**TGATAGACGCCACAGA**GGGG**CAGAGAGCAATCATCACCTGCA  
V3 V4 V5  
 AACCCCTCTATACTCACATCTACCAGTGTACGAATTGCATTAGAAAATGTTGC  
 ATTCAAAAATAGGTAGCATACAATTAAAACA**TGGCGG**GCACGTATCATTGCCCTATCT  
V6 V7  
 TGTGCAGTTAGACCGAATTTCGAAGAAGTACCTTCAAAGAA**TGGGGT**CTCATCTT  
V8  
 GTTTGCAAGTACCACTGAGC**AGG**ATAATAAGAAATGATAATACTATAGAGA  
V9  
 TAACGTCGATGACTCCCATACTGTAATTGCTTTAGTTGTATTAGTGCAAG  
 TTTCTGAAATCGATTAATTTCCTTCTTTATTAAACCTTAATTTCATTAA  
 GATTCTGACTTCAACTCAAGACGCACAGATATTATAACATCTGCACAATAGGCATTG  
 CAAGAATTACTCGTGAGTAAGGAAAGAGTGAGGAACATCGCATACTGCATTAAA  
 GATGCCGATT**TGGCGCGA**ATCCTTATTGGCTTCACCCTCATACTATTATC**AGGG**  
V10 V11  
 CAGAAAA**AGG**AAGTGTTCCTCCTCTGAATTGATGTTACCTCATAAGCACGTG  
V12  
 GCCTCTATCGAGAAAGAAATTACCGTCGCTCGTATTGTTGCAAAAAGAACAAA  
 ACTGAAAAAACCCAGACACGCTCGACTCCTGTCTTCTATTGATTGCAGCTTCCAAT  
 TTCGTCACACA**ACAGG**TCCTAGCGA**CGG**CTCAC**AGG**TTTGTAACAAGCAATCGAA  
V13 V14 V15

GGTTCTGGAA**TGGCGG**GAAAGGGTTAGTACCACATGCTATGATGCCACTGTGATCT  
**V16 V17**  
 CCAGAGCAAAGTCGTCGATCGTACTGTTACTCTCTCTTCAAACAGAACATTGTCC  
  
 GAATCGTGTGACAACAACAGCCTGTTCTCACACACTCTTCTTAACCA**AGGGGG**  
**V18 V19**  
 TGGTTAGTTAGTAGAACCTCGTGAAACTACATTACATATATAAACTTGCATAAA  
  
**TTGG**CAATGCAAGAAATACATATTGGTCTTCTAATTCTAGTTCAAGTTCTTA  
**V20**  
 GATGCTTCTTTCTCTTTACAGATCATCA**AGGAAGTAATTATCTACTTTACAA**  
**V21**  
 CAAATATAAAAACA**ATGTCTAAAGGTGAAGAATTATTCAC****TGG**TGTTGCCAATT**TG**  
**V22** **V23**  
**GT**TGAATTAGAT**TGG**TGATGTTA**TGG**TCACAAATTCTGTCTCC**CGGTGAAGGTGAA**  
**V24** **V25** **V26** **V27**  
 GGTGATGCTACTTACGGTAAATTGACCTAAAATTGATTGTACTAC**TGG**TAAATTGCC  
**V28**  
 AGTTCCATGGCCAACCTTAGTCACTACTT**AGGTTATGG**TTGCAATGTTTGCTAGAT  
**V29** **V30**  
 ACCCAGATCATATGAAACAACATGACTTTCAAGTCTGCCATGCCAGA**AGGTTATGT**  
**V31**  
 TCAAGAAAGAACTATTTTCAAAGATGAC**CGG**TAACTACAAGACCAGAGCTGAAGT  
**V32**  
 CAAGTTGAAGGTGATACCTTAGTTAATAGAATCGAATTAAA**AGG**TATTGATTAAAG  
**V33**  
 AAGA**TGG**TAACATTTAGGTACAAATTGGAATACAACACTATAACTCTCACAAATGTTAC  
**V34**  
 ATCACTGCTGACAAACAAAAGAATGGTATCAAAGCTAACTCAAAATTAGACACAAAC  
  
 ATTGAAGATGGTGGTGTCAATTAGCTGACCATTATCAACAAAATCTCAATTGGTG  
  
 ATGGTCCAGTCTGTTACCAAGACAACCATTACTTATCCTATCAATCTGCCATTCCAAA  
  
 GATCCAACGAAAAGAGAGACCACATGGTCTTGTAGAATTGTTACTGCTGCTGGTA  
  
 TTACCCATGGTATGGATGAATTGTACAAA

No.	Location	GC%	Energy	AGG	TGG	CGG	GGG	#G	#A	Fold change (log2)
V1	-1200	0.4	-13.6	0	1	0	0	5	2	0.18
V2	-1199	0.35	-13.9	0	0	0	1	4	2	0.42
V3	-1172	0.4	-12.6	0	0	1	0	1	3	0.11
V4	-1152	0.6	-12.3	0	0	0	1	6	6	0.07
V5	-1151	0.6	-12.1	0	0	0	1	7	6	0.60
V6	-1037	0.3	-7	0	1	0	0	3	10	0.05
V7	-1034	0.3	-7.9	0	0	1	0	3	10	0.24
V8	-965	0.35	-10.2	0	1	0	0	4	10	0.15
V9	-930	0.45	-8.9	1	0	0	0	4	5	0.22

V10	-645	0.35	-12.7	0	1	0	0	4	6	0.82
V11	-601	0.35	-7.7	1	0	0	0	0	5	0.27
V12	-589	0.4	-7	1	0	0	0	4	8	0.40
V13	-409	0.4	-7	1	0	0	0	1	7	0.01
V14	-397	0.5	-7	0	0	1	0	4	8	0.61
V15	-389	0.65	-10.3	1	0	0	0	6	4	0.51
V16	-356	0.45	-8.5	0	1	0	0	6	7	0.68
V17	-353	0.45	-9.6	0	0	1	0	7	6	0.63
V18	-199	0.35	-8.7	1	0	0	0	0	5	1.33
V19	-196	0.4	-9	0	0	0	1	2	4	0.51
V20	-132	0.15	-8.2	0	1	0	0	1	10	0.24
V21	-39	0.3	-7.1	1	0	0	0	1	5	1.71
V22	27	0.3	-12	0	1	0	0	4	9	-0.29
V23	44	0.45	-11	0	1	0	0	4	3	0.10
V24	57	0.3	-7.8	0	1	0	0	4	6	-1.82
V25	69	0.3	-7	0	1	0	0	6	7	-1.21
V26	90	0.4	-8.4	0	0	1	0	3	4	-0.17
V27	96	0.4	-9.5	1	0	0	0	4	4	0.21
V28	150	0.2	-8.6	0	1	0	0	2	7	-0.06
V29	192	0.4	-11.1	1	0	0	0	1	5	-1.66
V30	198	0.3	-7	0	1	0	0	3	5	-0.09
V31	270	0.5	-9.9	1	0	0	0	4	5	-0.27
V32	309	0.2	-8	0	0	1	0	2	7	0.09
V33	378	0.2	-7.1	1	0	0	0	3	10	-0.13
V34	399	0.25	-7.9	0	1	0	0	5	8	-0.49

**Table S4.** Key parameters of guide RNAs used in validation experiments (Eno2p-tdTomato).

CGCTCAGCATCTGCTTCTTCCAAAGATGAACG**CGG**CGTTATGTCACTAACGACGTGC  
T1  
ACCAACTTG**CGG**AAAG**TGG**ATCCC**GT**CCAAA**ACT****TGG**CATCC**CTA**ATTGATA**CA**TCT  
T2 T3 T4  
ACACACCGCACGC**CT**TTCTGAAGCCC**ACT****TCG****TGG**ACTTG**CC**ATATG**CAA**AT  
T5  
TCATGAAGTGTGATA**CC**AAGTCAG**CAT**ACAC**CT**CACT**AGG**TAGTT**CTT****TGG**TTGTA  
T6 T7  
TTGATCATT**TGG**TCATCG**TGG**TT**C**ATTAATTT**TTT**CT**CC**ATTG**C**TT**TGG**CTTGAT  
T8 T9 T10  
CTTACTATCATT**TGG**ATTT**TG**TCGA**AGG**TT**G**TAGAATTGTATGTGACAAG**TGG**CACCA  
T11 T12 T13  
AGCATATATAAAAAAAAAGCATTAT**CT****CC**ACC**AG**AGTTGATTGTTAAAAACGTAT  
TTATAGCAAACG**CA**ATTG**TA**ATT**AA**ATT**CT**TATT**TT**GTAT**CT****TT**CT**CC**GT**CT**CAATC  
TTT**TT**ATT**TT**ATT**TT**ATT**TT**CT**TT**CT**TT**AG**TT**CT**TT**CATAAC**AC**CAAG**CA**ACT**AA**ACT  
ATAACATACAATA**AT****GG**TGAG**CA**AGGG**CG**AGGAG**GT**CAT**AA**AGAG**TT**CAT**GCG**  
CTTCAAGGTGCG**CA****TGG****AGG**G**CT****CC****AT****GA****AC****CGG****CC****AC****G****AG****TT****CG****AG****AT****CG****AGG****CG**  
T14 T15 T16 T17 T18  
**AGGG****CG****AGGG****CC****CC****CT****AC****G****AGG****CC****AC****CC****AG****CC****GC****CA****AG****CT****GA****AG****GT****GA****CC****AA**  
T19 T20 T21 T22 T23 T24 T25 T26  
**GGG****CG****GG****CC****CC****CT****GC****CC****TT****CG****CT****GG****AC****AT****CC****GT****CC****CC****CC****AG****TT****C****AT****GT****TA****CGG****CT****CC**  
T27 T28 T29 T30  
AAGGCGTACGTGAAGC**AC****CC****CG****CC****AC****AT****CC****CG****ATT****AC****AA****AG****CT****GT****CC****TT****CC**  
**GAGG****G****CT****CA****AG****TGG****G****AG****CG****CG****GT****G****A****C****TT****CG****AG****G****CG****CG****GT****TGG****TG****AC****CG**  
T31 T32 T33 T34 T35 T36  
GACCCAGGACT**CC****CC****CT****GC****AG****GA****CG****GA****CG****CT****G****A****T****CA****AG****GT****GA****AG****AT****GC****CG**  
T37 T38 T39 T40  
CACCAACT**CC****CC****CC****CC****GA****CG****CC****CC****GT****AT****GC****AG****AA****AG****AC****CA****T****GGG****CT****GGG****AG**  
T41 T42 T43 T44 T45  
CCTCCACCGAG**GC****CC****CT****GT****AC****CC****CC****CG****GA****CG****CG****GT****GT****GA****AG****GG****GC****GA****GT****CC****AC****CC**  
T46 T47 T48  
**G****CC****CT****GA****AG****CT****GA****AG****GG****AC****GG****CG****GG****CC****AC****T****AC****CT****GG****GA****GT****TC****AA****AG****AC****CA****AT****CT****AC****A**  
T49  
**G****CC****AA****AG****CC****CG****GT****CA****AC****T****GC****CC****GG****CT****A****T****AC****AC****GT****GG****AC****AC****CA****AG****C****TGG****AC****AT**  
T50  
ACCTCCCACA**AC****CG****AG****G****ACT****A****CC****AC****AT****CG****TGG****AA****C****A****G****T****A****C****G****A****G****C****G****C**  
T51 T52 T53  
CCACCAC**CT****GT****TC****CT****GG****GC****AT****GG****CA****CC****GG****C****AG****CC****GG****C****AG****CG****CT****CC****GG****CA**  
T54 T55 T56 T57 T58 T59  
CCGC**CT****CC****CC****CG****AG****G****AC****AA****CA****AC****AT****TGG****CC****GT****C****AT****CA****AA****AG****AG****GT****TC****AT****GC****GT****CT****CA****AG**  
T60 T61  
TGC**GC****AT****TGG****AG****GG****CT****CC****AT****GA****AC****GG****CC****AC****G****AG****TT****CG****AG****AT****CG****AG****GG****GC****AG****GG****GC****AG**  
T62 T63 T64 T65 T66  
**G****CC****GC****CC****CT****AC****CG****AG****GG****CA****CC****AG****AC****CG****CC****AA****AG****CT****GA****AG****GT****AC****CA****AG****GG****CG****GG****CC**

T67 T68  
 CCTGCCCTCGCC **TGGG**ACATCCTGTCCCCCAGTTCATGTAC**GG**CTCCA **AGGC**TAC  
 T73T74 T69 T70T71 T72  
 GTGAAGCACCCCGCCGACATCCCCGATTACAAGAAGCTGTCCCTCCCCG **AGGG**CTTC  
 T77T78  
 AAG**TGGG**AGCGCGTGATGAACCTCG **AGG**AC**GG**CGGTCT**GG**TGACC**GT**GAC**CC****AGGA**  
 T79T80 T81 T82 T83 T84 T85  
 CTCCTCCCTGCAGGA **CGG**CACGCTGATCTACAAGGTGAAGATGCGCGGCACCAACTT  
 T86  
 CCCCCCGA**CGG**CCCCGTAATGCAGAAAGAACCATGGGCT**GGGAGG**CCTCCACCG  
 T87 T88 T89  
 AGCGCCTGTACCCCCGCGACGGCGTGCTGA **AGGG**CGAGATCCACC**AGG**CCCTGAAG  
 T90T91 T92  
 CTGA**AGG**A**CGGCGG**CCACTACCT**TGG**TGGAGTTCAAGACCATCTACATGCCAAGAAG  
 T93 T94 T95 T96  
 CCCGTGCAACTGCCCGGCTACTACTACGTGGACACCAAGCT**GG**ACATCACCTCCCAC  
 T97  
 AACG**AGG**ACTACACCACGT**TGG**AACAGTACGAGCGCTCCGAGGGCCGCCACCACT  
 T98 T99  
 GTTCCTGTACGGCATGGACGAGCTGTACAAG

No.	Location	GC%	Energy	AGG	TGG	CGG	GGG	#G	#A	Fold change (log2)
T1	-516	0.45	-7.9	0	0	1	0	3	6	-1.81
T2	-482	0.5	-8.6	0	0	1	0	4	6	0.59
T3	-475	0.55	-9.8	0	1	0	0	6	6	-1.79
T4	-456	0.5	-11.7	0	1	0	0	4	6	-1.85
T5	-397	0.45	-14.3	0	1	0	0	3	3	-1.86
T6	-338	0.45	-7.9	1	0	0	0	2	7	-1.67
T7	-325	0.45	-12.8	0	1	0	0	4	3	-1.53
T8	-308	0.3	-11.2	0	1	0	0	4	3	0.10
T9	-298	0.35	-7.8	0	1	0	0	4	4	-0.97
T10	-266	0.3	-7	0	1	0	0	1	1	-1.12
T11	-244	0.3	-10	0	1	0	0	2	4	-0.15
T12	-230	0.3	-8	1	0	0	0	4	4	-1.94
T13	-205	0.35	-8.4	0	1	0	0	6	7	-1.72
T14	56	0.6	-15.8	0	1	0	0	6	4	-1.41
T15	59	0.65	-14.4	1	0	0	0	8	3	-1.62
T16	72	0.6	-14.9	0	0	1	0	7	5	-1.43
T17	92	0.65	-9.7	1	0	0	0	7	4	-2.29
T18	93	0.6	-9.3	0	0	0	1	7	5	-1.36
T19	98	0.65	-12.7	1	0	0	0	9	4	-1.94
T20	99	0.6	-10.6	0	0	0	1	9	5	-1.90
T21	104	0.75	-10.8	1	0	0	0	11	4	-2.27
T22	105	0.7	-8.7	0	0	0	1	11	5	-1.79
T23	119	0.85	-16.2	1	0	0	0	9	2	-2.11
T24	120	0.8	-12.8	0	0	0	1	8	3	-1.98

T25	143	0.65	-8.3	1	0	0	0	4	6	-2.41
T26	152	0.6	-11.2	1	0	0	0	6	6	-2.15
T27	153	0.55	-10.2	0	0	0	1	6	7	-1.74
T28	156	0.55	-9.5	0	0	1	0	8	7	-1.25
T29	176	0.8	-10.9	0	0	0	1	4	0	-1.65
T30	204	0.55	-7.4	0	0	1	0	3	3	-2.16
T31	269	0.6	-9.8	1	0	0	0	4	4	-2.20
T32	270	0.55	-10.1	0	0	0	1	4	5	-2.19
T33	280	0.65	-11.1	0	1	0	0	5	3	-1.77
T34	302	0.6	-8.8	1	0	0	0	8	4	0.10
T35	306	0.55	-9.3	0	0	1	0	7	5	-0.13
T36	314	0.65	-11.8	0	1	0	0	8	4	-2.07
T37	344	0.7	-11.5	1	0	0	0	4	3	-1.39
T38	348	0.65	-14.4	0	0	1	0	5	4	-0.44
T39	365	0.6	-8.9	1	0	0	0	6	5	-0.28
T40	378	0.45	-8.7	0	0	1	0	6	7	-0.12
T41	399	0.7	-8.6	0	0	1	0	3	4	0.33
T42	425	0.45	-7	0	1	0	0	5	9	-0.42
T43	426	0.4	-9.7	0	0	0	1	5	9	0.68
T44	430	0.55	-7	0	1	0	0	7	7	0.70
T45	434	0.6	-9	1	0	0	0	9	6	-0.60
T46	465	0.75	-8.9	0	0	1	0	6	3	-1.75
T47	476	0.8	-11	1	0	0	0	7	2	0.68
T48	491	0.65	-10.4	1	0	0	0	7	5	-0.65
T49	548	0.45	-7	0	1	0	0	4	7	0.24
T50	599	0.55	-7.8	0	1	0	0	4	6	-1.09
T51	620	0.6	-7.9	1	0	0	0	3	6	-0.55
T52	635	0.55	-8.2	0	1	0	0	4	7	-0.77
T53	657	0.6	-8.4	0	0	0	1	6	6	-0.34
T54	679	0.7	-10.1	0	0	0	1	4	2	-2.56
T55	684	0.65	-10.3	0	1	0	0	5	3	-2.05
T56	690	0.65	-9.5	0	0	1	0	7	2	-2.33
T57	699	0.75	-9.7	0	0	1	0	8	4	-2.55
T58	705	0.8	-12.5	0	0	1	0	8	4	-2.74
T59	714	0.75	-12	0	0	1	0	7	4	-2.49
T60	731	0.8	-11	1	0	0	0	4	1	-2.14
T61	743	0.55	-9.7	0	1	0	0	3	7	-2.25
T62	782	0.6	-15.8	0	1	0	0	6	4	-2.48
T63	786	0.6	-9.6	0	0	0	1	7	4	-2.37
T64	818	0.65	-9.7	1	0	0	0	7	4	-2.37
T65	824	0.65	-12.7	1	0	0	0	9	4	-2.10
T66	830	0.75	-10.8	1	0	0	0	11	4	-1.65
T67	845	0.85	-16.2	1	0	0	0	9	2	-0.04
T68	846	0.8	-12.8	0	0	0	1	8	3	-0.17
T69	869	0.65	-8.3	1	0	0	0	4	6	0.03

T70	878	0.6	-11.2	1	0	0	0	6	6	-0.30
T71	879	0.55	-10.2	0	0	0	1	6	7	-0.98
T72	882	0.55	-9.5	0	0	1	0	8	7	-0.08
T73	901	0.85	-10.6	0	1	0	0	5	0	-0.07
T74	902	0.8	-10.9	0	0	0	1	4	0	-1.79
T75	930	0.55	-7.4	0	0	1	0	3	3	0.18
T76	938	0.55	-7.4	1	0	0	0	4	4	0.29
T77	995	0.6	-9.8	1	0	0	0	4	4	-1.08
T78	996	0.55	-10.1	0	0	0	1	4	5	0.01
T79	1006	0.65	-11.1	0	1	0	0	5	3	0.03
T80	1007	0.6	-9.4	0	0	0	1	5	3	-0.37
T81	1028	0.6	-8.8	1	0	0	0	8	4	-0.06
T82	1032	0.55	-9.3	0	0	1	0	7	5	0.16
T83	1035	0.55	-8.1	0	0	1	0	8	5	0.26
T84	1040	0.65	-11.8	0	1	0	0	8	4	0.10
T85	1055	0.7	-14.3	1	0	0	0	7	2	-0.90
T86	1074	0.65	-14.4	0	0	1	0	5	4	-0.36
T87	1125	0.7	-8.6	0	0	1	0	3	4	-0.38
T88	1157	0.55	-7.9	0	0	0	1	7	7	0.30
T89	1160	0.6	-9	1	0	0	0	9	6	0.35
T90	1202	0.8	-11	1	0	0	0	7	2	-0.29
T91	1203	0.75	-10.2	0	0	0	1	7	3	-0.15
T92	1217	0.65	-10.4	1	0	0	0	7	5	-0.20
T93	1232	0.65	-9.5	1	0	0	0	5	5	-0.32
T94	1236	0.6	-12.1	0	0	1	0	7	6	-0.28
T95	1239	0.65	-11.7	0	0	1	0	8	5	0.14
T96	1250	0.7	-10.8	0	1	0	0	7	5	-0.01
T97	1325	0.55	-7.8	0	1	0	0	4	6	-2.05
T98	1346	0.6	-7.9	1	0	0	0	3	6	-1.95
T99	1361	0.55	-8.2	0	1	0	0	4	7	-1.96

**Table S5.** Binary regression decision tree model.

Group	Value	Decision path	Decision nodes
1	0.115	<6 → <4 → <-563	GC%
2	-0.871	<6 → <4 → ≥-563	#G
3	2.122	<6 → ≥4 → ≥-13.45	aLoc
4	-1.044	<6 → ≥4 → ≥-13.45 → <-408 → ≥-528	#A
5	0.821	<6 → ≥4 → ≥-13.45 → <-408 → <-528 → <-12.5	ΔG
6	0.597	<6 → ≥4 → ≥-13.45 → <-408 → <-528 → ≥-12.5 → ≥7	TGG
7	0.018	<6 → ≥4 → ≥-13.45 → <-408 → <-528 → ≥-12.5 → <7 → <-8.1	GGG
8	0.240	<6 → ≥4 → ≥-13.45 → <-408 → <-528 → ≥-12.5 → <7 → ≥-8.1	AGG
9	2.364	<6 → ≥4 → ≥-13.45 → >-408 → <-404	CGG
10	0.053	<6 → ≥4 → ≥-13.45 → >-408 → ≥-404 → <4 → ≥7	
11	0.564	<6 → ≥4 → ≥-13.45 → >-408 → ≥-404 → <4 → <7 → <-8.4	
12	2.323	<6 → ≥4 → ≥-13.45 → >-408 → ≥-404 → <4 → <7 → ≥-8.4	
13	-0.755	<6 → ≥4 → ≥-13.45 → >-408 → ≥-404 → ≥4 → <8.45	
14	-0.401	<6 → ≥4 → ≥-13.45 → >-408 → ≥-404 → ≥4 → <-8.45 → <-394	
15	0.526	<6 → ≥4 → ≥-13.45 → >-408 → ≥-404 → ≥4 → <-8.45 → ≥-394	
16	-3.382	≥6 → <-9.15 → <838 → <0.525 → <18	
17	0.319	≥6 → <-9.15 → <838 → <0.525 → ≥18 → =1	
18	0.055	≥6 → <-9.15 → <838 → <0.525 → ≥18 → =0 → <4	
19	-0.400	≥6 → <-9.15 → <838 → <0.525 → ≥18 → =0 → <4 → ≥5	
20	-0.542	≥6 → <-9.15 → <838 → <0.525 → ≥18 → =0 → <4 → ≥4 → <5 → ≥0.275	
21	-1.662	≥6 → <-9.15 → <838 → <0.525 → ≥18 → =0 → <4 → ≥4 → <5 → ≥0.275 → <3	
22	-1.097	≥6 → <-9.15 → <838 → <0.525 → ≥18 → =0 → <4 → ≥4 → <5 → ≥0.275 → <3 → <-13.7	
23	-0.606	≥6 → <-9.15 → <838 → <0.525 → ≥18 → =0 → <4 → ≥4 → <5 → ≥0.275 → <3 → <-13.7 → <-12.5	
24	-0.925	≥6 → <-9.15 → <838 → <0.525 → ≥18 → =0 → <4 → ≥4 → <5 → ≥0.275 → <3 → <-13.7 → <-12.5 → <341	
25	-0.596	≥6 → <-9.15 → <838 → <0.525 → ≥18 → =0 → <4 → ≥4 → <5 → ≥0.275 → <3 → <-13.7 → <-12.5 → ≥341	
26	-0.134	≥6 → <-9.15 → <838 → <0.525 → <585 → ≥346	
27	-0.484	≥6 → <-9.15 → <838 → <0.525 → <585 → <346 → <2	
28	-0.911	≥6 → <-9.15 → <838 → <0.525 → <585 → <346 → ≥2 → ≥9.6	
29	-1.488	≥6 → <-9.15 → <838 → <0.525 → <585 → <346 → ≥2 → <9.6 → <82	
30	-1.706	≥6 → <-9.15 → <838 → <0.525 → <585 → <346 → ≥2 → <9.6 → ≥82 → <4	
31	-2.083	≥6 → <-9.15 → <838 → <0.525 → <585 → <346 → ≥2 → <9.6 → ≥82 → ≥4	
32	-1.654	≥6 → <-9.15 → <838 → <0.525 → ≥585 → ≥827	
33	-2.290	≥6 → <-9.15 → <838 → <0.525 → ≥585 → <827 → =0	
34	-2.528	≥6 → <-9.15 → <838 → <0.525 → ≥585 → <827 → =1	
35	-0.953	≥6 → <-9.15 → <838 → <5	
36	-0.009	≥6 → <-9.15 → <838 → ≥5 → ≥8	
37	-0.980	≥6 → <-9.15 → <838 → ≥5 → <8 → ≥7	
38	-0.628	≥6 → <-9.15 → <838 → ≥5 → <8 → <7 → <-13.2	
39	0.157	≥6 → <-9.15 → <838 → ≥5 → <8 → <7 → ≥-13.2 → ≥-9.4	
40	-0.273	≥6 → <-9.15 → <838 → ≥5 → <8 → <7 → ≥-13.2 → ≥-9.4 → =0	
41	-0.018	≥6 → <-9.15 → <838 → ≥5 → <8 → <7 → ≥-13.2 → ≥-9.4 → =1	
42	-1.983	≥6 → <-9.15 → ≥1243	
43	0.028	≥6 → <-9.15 → <1243 → <147 → ≥8	
44	-2.099	≥6 → <-9.15 → <1243 → <147 → <8 → ≥0.575	
45	-0.604	≥6 → <-9.15 → <1243 → <147 → <8 → <0.575 → <5	
46	-1.196	≥6 → <-9.15 → <1243 → <147 → <8 → <0.575 → ≥5	
47	-1.242	≥6 → <-9.15 → <1243 → <147 → <4	
48	0.193	≥6 → <-9.15 → <1243 → <147 → <4 → ≥1	
49	0.324	≥6 → <-9.15 → <1243 → <147 → <4 → ≥1 → <-7.5 → =0	
50	0.036	≥6 → <-9.15 → <1243 → <147 → <4 → ≥1 → <-7.5 → =0 → <1141 → <6	

**Cont. Table S5.** Binary regression decision tree model.

Group	Value	Decision path
51	-0.206	(Yellow) $\geq 6$ → (Orange) $\geq -9.15$ → (Yellow) $< 1243$ → (Yellow) $\geq 147$ → (Orange) $\geq 4$ → (Green) $\geq 1$ → (Orange) $< -7.5$ → (Red) $= 0$ → (Yellow) $< 1141$ → (Orange) $\geq 6$ → (Green) $< 8$
52	-0.605	(Yellow) $\geq 6$ → (Orange) $\geq -9.15$ → (Yellow) $< 1243$ → (Yellow) $\geq 147$ → (Orange) $\geq 4$ → (Green) $\geq 1$ → (Orange) $< -7.5$ → (Red) $= 0$ → (Yellow) $< 1141$ → (Orange) $\geq 6$ → (Green) $\geq 8$
53	-0.209	(Yellow) $\geq 6$ → (Orange) $\geq -9.15$ → (Yellow) $< 1243$ → (Yellow) $\geq 147$ → (Orange) $\geq 4$ → (Green) $\geq 1$ → (Orange) $< -7.5$ → (Red) $= 1$ → (Yellow) $< 441$
54	-0.745	(Yellow) $\geq 6$ → (Orange) $\geq -9.15$ → (Yellow) $< 1243$ → (Yellow) $\geq 147$ → (Orange) $\geq 4$ → (Green) $\geq 1$ → (Orange) $< -7.5$ → (Red) $= 1$ → (Yellow) $\geq 441$
55	0.511	(Yellow) $\geq 6$ → (Orange) $\geq -9.15$ → (Yellow) $< 1243$ → (Yellow) $\geq 147$ → (Orange) $\geq 4$ → (Green) $\geq 1$ → (Orange) $> -7.5$ → (Green) $\geq 0.475$
56	0.671	(Yellow) $\geq 6$ → (Orange) $\geq -9.15$ → (Yellow) $< 1243$ → (Yellow) $\geq 147$ → (Orange) $\geq 4$ → (Green) $\geq 1$ → (Orange) $> -7.5$ → (Green) $< 0.475$ → (Red) $= 1$
57	0.158	(Yellow) $\geq 6$ → (Orange) $\geq -9.15$ → (Yellow) $< 1243$ → (Yellow) $\geq 147$ → (Orange) $\geq 4$ → (Green) $\geq 1$ → (Orange) $> -7.5$ → (Green) $< 0.475$ → (Red) $= 0$ → (Yellow) $\geq 498$
58	0.178	(Yellow) $\geq 6$ → (Orange) $\geq -9.15$ → (Yellow) $< 1243$ → (Yellow) $\geq 147$ → (Orange) $\geq 4$ → (Green) $\geq 1$ → (Orange) $> -7.5$ → (Green) $< 0.475$ → (Red) $= 0$ → (Yellow) $\geq 498$ → (Red) $= 1$
59	-0.067	(Yellow) $\geq 6$ → (Orange) $\geq -9.15$ → (Yellow) $< 1243$ → (Yellow) $\geq 147$ → (Orange) $\geq 4$ → (Green) $\geq 1$ → (Orange) $> -7.5$ → (Green) $< 0.475$ → (Red) $= 0$ → (Yellow) $\geq 498$ → (Red) $= 0$ → (Yellow) $\geq 498$ → (Red) $= 0$ → (Orange) $\leq -7.15$
60	-0.252	(Yellow) $\geq 6$ → (Orange) $\geq -9.15$ → (Yellow) $< 1243$ → (Yellow) $\geq 147$ → (Orange) $\geq 4$ → (Green) $\geq 1$ → (Orange) $> -7.5$ → (Green) $< 0.475$ → (Red) $= 0$ → (Yellow) $\geq 498$ → (Red) $= 0$ → (Yellow) $\geq 498$ → (Red) $= 0$ → (Orange) $\geq -7.15$

**Table S6.** Measured and predicted concentrations of products from violacein pathway

Strains	Measured concentrations (A.U.)				Predicted concentrations (A.U.)			
	PV	PDV	V	DV	PV	PDV	V	DV
TEF1p(H)	472.00	216.30	229.70	22.90	481.83	219.39	220.37	27.13
TEF1p(M)	392.70	206.80	294.00	32.30	422.47	191.06	191.92	24.63
TEF1p(L)	345.70	138.30	177.00	16.30	356.13	159.59	160.32	21.71
PDC1p(H)	408.30	188.60	222.50	23.50	835.91	390.75	392.48	40.50
PDC1p(M)	297.30	142.80	168.70	2.10	417.21	188.55	189.41	24.41
PDC1p(L)	55.10	40.70	60.70	0.10	85.92	35.23	35.40	7.36
TPI1p(M)	270.00	134.20	120.70	14.20	537.68	102.32	200.50	25.40
TPI1p(L)	342.20	120.00	132.90	15.90	239.27	400.73	200.50	25.40
ENO2p(H)	375.20	168.60	147.10	17.40	357.22	192.65	283.68	32.35
ENO2p(M)	337.80	156.20	199.20	19.90	425.71	198.31	215.19	26.69
ENO2p(L)	455.60	231.70	74.30	24.70	598.05	216.54	42.85	8.46
ACD	235.15	161.80	251.65	34.20	57.17	363.64	295.96	36.48
CD	219.75	149.10	245.45	28.10	57.17	297.88	295.96	36.48
AD	251.95	286.35	81.10	23.40	202.19	377.62	150.95	22.50

Note: PV: Proviolacein, PDV: Prodeoxyviolacein, V: Violacein, DV: Deoxyviolacein